POLITECNICO DI TORINO
Repository ISTITUZIONALE

Magneto-electro-elastic 3D coupling in free vibrations of layered plates

Original
Magneto-electro-elastic 3D coupling in free vibrations of layered plates / Brischetto, S., Cesare, D., Mondino, T.. - In: COMPUTERS, MATERIALS & CONTINUA. - ISSN 1546-2218. - 85:3(2025), pp. 4491-4518. [10.32604/cmc.2025.068518]

Availability:
This version is available at: 11583/3004429 since: 2025-10-24T09:02:01Z

Publisher:
Tech Science Press

Published
DOI:10.32604/cmc.2025.068518

Terms of use:

This article is made available under terms and conditions as specified in the corresponding bibliographic description in the repository

Publisher copyright

(Article begins on next page)

26 November 2026

Computers, Materials & Continua

Tech Science Press

Doi:10.32604/cmc.2025.068518

ARTICLE

Magneto-Electro-Elastic 3D Coupling in Free Vibrations of Layered Plates

Salvatore Brischetto*, Domenico Cesare and Tommaso Mondino

Department of Mechanical and Aerospace Engineering, Politecnico di Torino, Torino, 10129, Italy

*Corresponding Author: Salvatore Brischetto. Email: salvatore.brischetto@polito.it

Received: 30 May 2025; Accepted: 03 September 2025; Published: 23 October 2025

ABSTRACT: A three-dimensional (3D) analytical formulation is proposed to put together magnetic, electric and elastic fields to analyze the vibration modes of simply-supported layered piezo-electro-magnetic plates. The present 3D model allows analyses for layered smart plates in both open-circuit and closed-circuit configurations. The second-order differential equations written in the mixed curvilinear reference system govern the magneto-electro-elastic free vibration problem for multilayered plates. This set consists of the 3D equations of motion and the 3D divergence equations for the magnetic induction and electric displacement. Navier harmonic forms in the planar directions and the exponential matrix method in the transversal direction of the plate are applied to solve the second-order differential equations in terms of displacements. For these reasons, simply-supported boundary conditions are considered. Imposition of interlaminar continuity conditions on primary variables (displacements, magnetic potential, electric potential), and some secondary variables (transverse normal and transverse shear stresses, transverse normal magnetic induction/electric displacement) allows the implementation of the layer-wise approach. Assessments for both load boundary configurations are proposed in the results section to validate the present 3D approach. 3D electro-elastic and 3D magneto-elastic coupling validations are performed separately considering different models from the open literature. A new benchmark involving a full magneto-electro-elastic coupling for multilayered plates is presented considering both load boundary configurations for different thickness ratios. For this benchmark, circular frequency values and related vibration modes through the transverse direction in terms of displacements, magnetic and electric potential, transverse normal magnetic induction/electric displacement are shown to visualize the magneto-electro-elastic coupling and material and thickness layer effects. The present formulation has been entirely implemented in an academic Matlab (R2024a) code developed by the authors. In this paper, for the first time, the second-order differential equations governing the magneto-electro-elastic problem for the free vibration analysis of plates has been solved considering the mixed mode of harmonic forms and exponential matrix. The exponential matrix permits computing the secondary variable of the problem (stresses, electric displacement components and magnetic induction components) exactly, directly from constitutive and geometrical equations. In addition, the very simple and elegant formulation permits having a code with very low computational costs. The present manuscript aims to fill the void in open literature regarding reference 3D solutions for the free vibration analysis of magneto-electro-elastic plates.

KEYWORDS: 3D analytical formulation; multilayered smart plates; free vibration analyses; vibration modes; magneto-electro-elastic coupling; exponential matrix method; layer wise approach

1 Introduction

Magneto-electro-elastic (MEE) structures are smart structures where the energy between all the involved fields is exchanged interacting each other [1–3]. This ability (called MEE coupling) is employed in smart structures for the health monitoring and for the suppression of unwanted vibrations [4,5]. For these

Copyright © 2025 The Authors. Published by Tech Science Press.
This work is licensed under a Creative Commons Attribution 4.0 International License, which permits unrestricted use, distribution, and reproduction in any medium, provided the original work is properly cited.

reasons, researchers are interested in analytical and numerical tool developments for the analysis of these types of smart structures. Several analytical and numerical models have been developed in the open literature to understand smart structure behaviors [6,7].

In the framework of numerical models, Carrera et al. [8] developed refined finite elements for multilayered plates subjected to MEE fields. The natural characteristics of a three-layered simply supported MEE multilayered plate were studied by Yang et al. in [9]. In [10], a free vibration study for anisotropic functionally graded MEE plates was carried out using a semi-analytical finite element method based on the series solution in the in-plane directions of the plate and on the finite element approximation through the thickness direction of the structure. Chen et al. [11] presented a free vibration study of multilayered MEE plates, under combined clamped/free lateral boundary conditions, by using a semi-analytical discrete-layer approach. Jiangong et al. [12] studied the dispersion behavior of waves in a layered MEE plate. Legendre orthogonal polynomial series were employed in controlling equations to include the MEE coupling. In [13], a finite element (FE) approach was proposed for free vibrations and transient peculiarities of MEE composite rectangular and elliptical plates resting on the visco-Pasternak medium in the case of a hygro-thermal environment and blast load applications. Kattimani and Ray [14] presented an FE model to analyze the active constrained layer damping for large amplitude vibrations of smart MEE plates. In [15], the nonlinear forced vibration behavior of MEE composite plates involving elastic foundations was studied via Reddy's third-order shear deformation theory. Vinyas [16] proposed the free vibration study of different carbon nanotube-reinforced MEE plates adopting FE methods and considering the higher-order shear deformation theory. Milazzo [17,18] proposed a variable kinematics approach for moderately large deflection analysis of smart MEE multilayered and functionally graded plates, 2D refined equivalent single-layer models were developed. The same author [19] also proposed an equivalent single-layer model for the free vibration analysis of smart laminated plates by considering quasi-static electric and magnetic fields. Davì and Milazzo [20] developed a regular variational boundary element formulation, based on a hybrid variational principle, for dynamic analyses of 2D MEE domains. Vinyas and Kattimani [21] discussed the effects of the hygrothermal environment on free vibration characteristics of MEE plates, the FE method and a higher order shear deformation theory were employed. Ramirez et al. [22] presented a free vibration approximate solution for the 2D MEE laminates in order to determine their fundamental behavior. In [23], a layerwise FE model was developed by Kiran and Kattimani using the shear deformation theory and coupled constitutive equations, non-dimensional eigenfrequencies of 3D multilayered MEE plates with skewed edges were computed.

In the case of analytical formulations for the free vibration study of MEE structures, Soni et al. [24] proposed a nonlinear analytical classical plate theory for transverse vibrations of cracked MEE thin plates. The material employed in this study was the reinforced $BaTiO_3$–$CoFe_2O_4$ composite including a central partial crack. In Xu et al. [25], the nonlinear free vibration response of MEE composite plates was proposed, the von Karman's nonlinear strain–displacement theory and the high-order shear deformation theory were employed. The bending and free vibrations of an MEE plate with surface effects were proposed in Yang and Li [26]. The governing differential equations for bending and vibrations of MEE plates were derived considering surface effects in the Kirchhoff thin plate theory. Chen et al. [27] presented a state-vector approach to detect free vibrations of MEE laminated plates. The same authors [28,29] developed a 3D analytical solution for the propagation of time-harmonic waves in transversely isotropic and multilayered MEE plates with nonlocal effects. Pan and Heyliger [30] presented an analytical solution for free vibrations of simply supported multilayered MEE rectangular plates; the Stroh formalism was used for the general solution. Dat et al. [31] developed an analytical solution for the nonlinear MEE vibrations of smart sandwich plates made of a carbon nanotube reinforced composite core embedded between two MEE face sheets. In Wang et al. [32], a state variable mixed type formulation was developed for the free vibration of laminated

structures embedding actuators/sensors. Razavi and Shooshtari [33] presented the nonlinear free vibration study of symmetric MEE laminated rectangular plates with simply supported boundary conditions, first-order shear deformation theory and von Karman's nonlinear strains were included in the model. A 3D semi-analytical solution of the elasticity theory was derived by Xin and Hu [34] for free vibrations of simply supported and multilayered MEE plates, the analysis combined the state space approach and the discrete singular convolution algorithm. Kuo and Wang [35] proposed an analysis for the investigation of wave motion characteristics (e.g., dispersion curves and mode shapes) for MEE laminated plates including generalized membrane-type interfacial imperfections. In Dinh and Duc [36], the vibration behavior of a honeycomb composite structure embedding electromagnetic layers was presented. Combined effects of uniform loadings, thermal stresses and electromagnetic potentials were investigated. The effect of the elastic foundation and the viscoelastic interface on the dynamic behaviour of laminated simply supported MEE rectangular plates was investigated by Hamidi et al. [37]. The state space method in the Laplace domain was used. Free vibrations of simply supported rectangular MEE nanoplates were studied in [38], the nonlocal Kirchhoff plate theory was employed. A buckling and free vibration model of MEE nanoplates was presented by Li et al. [39], nonlocal Mindlin theory resting on Pasternak foundation was implemented. Chang [40] investigated the free vibration behavior of fluid-loaded transversely isotropic MEE rectangular plates. In Jamalpoor et al. [41], free vibration and biaxial buckling of MEE microplates were shown. The Kelvin–Voigt visco-Pasternak foundation was implemented when initial external electric and magnetic potentials were applied. In [42], nonlinear forced vibrations of an immovable simply supported MEE rectangular plate were studied considering the first-order shear deformation theory and harmonic excitation forces.

The present 3D coupled MEE analytical approach for the free vibration analysis of open and closed circuit simply supported plates is employed to comprehend the behavior of layered smart structures for health monitoring and suppression of vibrations. The present 3D model consists of a set of five second-order differential equations. Navier harmonic forms in the planar directions and the exponential matrix in the transverse direction are applied. The exponential matrix in the thickness direction allows exact computations of stresses, strains, electric displacement components and magnetic induction components. This 3D formulation includes a layer-wise approach where congruence and equilibrium conditions are imposed at each layer interface. Displacements, electric potential, magnetic potential, stresses, transverse normal electric displacement and transverse normal magnetic induction are correctly evaluated by taking into account the zigzag effect. Brischetto and Cesare proposed 3D coupled electro-elastic free vibrations in [43] and 3D coupled magneto-elastic free vibrations in [44]. 3D pure elastic free vibration analysis of multilayered structures was proposed in [45]. For the first time, a 3D coupled magneto-electro-elastic free vibration analysis of layered plates is proposed considering the exponential matrix method in the transverse direction and the Navier harmonic forms in the planar directions. Results proposed in this paper can be used by scientists involved in the development of other formulations for magneto-electro-elastic analyses and by those researchers interested in the free vibration analysis of smart magneto-electro-elastic structures. The present paper is organized in different sections: in the second section, the 3D coupled magneto-electro-elastic model is presented in terms of governing, geometric and constitutive equations and solution methodology; in the third section, assessments are proposed to validate the model and new benchmark cases are shown to investigate the free vibration behavior of MEE multilayered plates. Some conclusive remarks and future developments are reported in the last section.

2 3D Magneto-Electro-Elastic Analytical Formulation

The present section shows the 3D formulation for coupled magneto-electro-elastic free vibration analyses of flat panels. In the first subsection, the set of five second-order differential governing equations

for the 3D magneto-electro-elastic coupling is proposed. Then, constitutive and geometrical relations are shown. In the last subsection discusses the solution method in terms of Navier harmonic forms in the planar directions and the exponential matrix in the transverse direction.

2.1 3D Set of Governing Equations for the Magneto-Electro-Elastic Plate Problem

The five 3D governing equations for the magneto-electro-elastic free vibration analysis can be explicitly written for each k layer included in multilayered flat panels:

$$\sigma^k_{xx,x} + \sigma^k_{xy,y} + \sigma^k_{xz,z} = \rho^k \ddot{u}^k, \tag{1a}$$

$$\sigma^k_{xy,x} + \sigma^k_{yy,y} + \sigma^k_{yz,z} = \rho^k \ddot{v}^k, \tag{1b}$$

$$\sigma^k_{xz,x} + \sigma^k_{yz,y} + \sigma^k_{zz,z} = \rho^k \ddot{w}^k, \tag{1c}$$

$$\mathcal{B}^k_{x,x} + \mathcal{B}^k_{y,y} + \mathcal{B}^k_{z,z} = 0, \tag{1d}$$

$$\mathcal{D}^k_{x,x} + \mathcal{D}^k_{y,y} + \mathcal{D}^k_{z,z} = 0. \tag{1e}$$

Stresses (σ^k_{xx}, σ^k_{xy}, σ^k_{xz}, σ^k_{yy}, σ^k_{yz}, σ^k_{zz}), magnetic inductions ($\mathcal{B}^k_x$, $\mathcal{B}^k_y$, $\mathcal{B}^k_z$) and electric displacements ($\mathcal{D}^k_x$, $\mathcal{D}^k_y$, $\mathcal{D}^k_z$) are dependent from coordinates x, y and z and time t. ρ^k indicates material mass density. $\ddot{u}^k$, $\ddot{v}^k$ and $\ddot{w}^k$ are displacements second derivatives in time. Subscripts $,x$, $,y$ and $,z$ state partial derivatives performed with respect to rectilinear coordinates. Eqs. (1d and 1e) have been derived in an orthogonal reference system using the work by Povstenko [46]; magnetic induction and electric displacement have been properly rewritten. The orthogonal rectilinear reference system and geometry defined for flat panels (plates) are clearly indicated in Fig. 1.

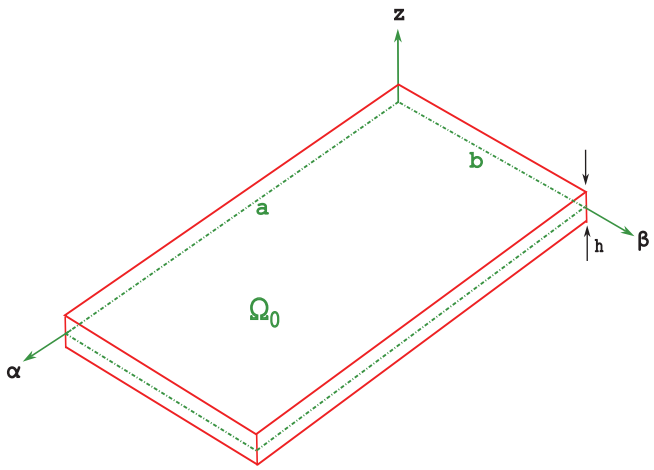

Figure 1: Plate (flat panel) geometry. Dotted green lines represent the Ω_0 middle reference surface

2.2 Geometrical and Constitutive Equations for the Magneto-Electro-Elastic Plate Problem

Geometrical equations are employed to link displacements with strains, the electric potential with the electric field and the magnetic potential with the magnetic field. MEE geometrical relations are:

$$\varepsilon^k_{xx} = u^k_{,x}, \quad \varepsilon^k_{yy} = v^k_{,y}, \quad \varepsilon^k_{zz} = w^k_{,z}, \tag{2a}$$

$$\gamma_{yz}^k = v_{,z}^k + w_{,y}^k, \quad \gamma_{xz}^k = u_{,z}^k + w_{,x}^k, \quad \gamma_{xy}^k = u_{,y}^k + v_{,x}^k, \tag{2b}$$

$$\mathcal{E}_x^k = -\phi_{,x}^k, \quad \mathcal{E}_y^k = -\phi_{,y}^k, \quad \mathcal{E}_z^k = -\phi_{,z}^k, \tag{3}$$

$$\mathcal{H}_x^k = -\psi_{,x}^k, \quad \mathcal{H}_y^k = -\psi_{,y}^k, \quad \mathcal{H}_z^k = -\psi_{,z}^k, \tag{4}$$

where ε_{xx}^k, ε_{yy}^k, ε_{zz}^k, γ_{yz}^k, γ_{xz}^k and γ_{xy}^k are strain components; $\mathcal{E}_x^k$, $\mathcal{E}_y^k$ and $\mathcal{E}_z^k$ are electric field components; ϕ^k is the electric potential; $\mathcal{H}_x^k$, $\mathcal{H}_y^k$ and $\mathcal{H}_z^k$ are magnetic field components; ψ^k is the magnetic potential.

Constitutive equations are employed to link stresses, the electric displacement and the magnetic induction with strains, electric field components and magnetic field components. Their explicit form is:

$$\sigma_{xx}^k = C_{11}^k\varepsilon_{xx}^k + C_{12}^k\varepsilon_{yy}^k + C_{13}^k\varepsilon_{zz}^k + C_{16}^k\gamma_{xy}^k - e_{31}^k\mathcal{E}_z^k - q_{31}^k\mathcal{H}_z^k, \tag{5a}$$

$$\sigma_{yy}^k = C_{12}^k\varepsilon_{xx}^k + C_{22}^k\varepsilon_{yy}^k + C_{23}^k\varepsilon_{zz}^k + C_{26}^k\gamma_{xy}^k - e_{32}^k\mathcal{E}_z^k - q_{32}^k\mathcal{H}_z^k, \tag{5b}$$

$$\sigma_{zz}^k = C_{13}^k\varepsilon_{xx}^k + C_{23}^k\varepsilon_{yy}^k + C_{33}^k\varepsilon_{zz}^k + C_{36}^k\gamma_{xy}^k - e_{33}^k\mathcal{E}_z^k - q_{33}^k\mathcal{H}_z^k, \tag{5c}$$

$$\sigma_{yz}^k = C_{44}^k\gamma_{yz}^k + C_{45}^k\gamma_{xz}^k - e_{14}^k\mathcal{E}_x^k - e_{24}^k\mathcal{E}_y^k - q_{14}^k\mathcal{H}_x^k - q_{24}^k\mathcal{H}_y^k, \tag{5d}$$

$$\sigma_{xz}^k = C_{45}^k\gamma_{yz}^k + C_{55}^k\gamma_{xz}^k - e_{15}^k\mathcal{E}_x^k - e_{25}^k\mathcal{E}_y^k - q_{15}^k\mathcal{H}_x^k - q_{25}^k\mathcal{H}_y^k, \tag{5e}$$

$$\sigma_{xy}^k = C_{16}^k\varepsilon_{xx}^k + C_{26}^k\varepsilon_{yy}^k + C_{36}^k\varepsilon_{zz}^k + C_{66}^k\gamma_{xy}^k - e_{36}^k\mathcal{E}_z^k - q_{36}^k\mathcal{H}_z^k, \tag{5f}$$

$$\mathcal{D}_x^k = e_{14}^k\gamma_{yz}^k + e_{15}^k\gamma_{xz}^k + \varepsilon_{11}^k\mathcal{E}_x^k + \varepsilon_{12}^k\mathcal{E}_y^k + d_{11}^k\mathcal{H}_x^k + d_{12}^k\mathcal{H}_y^k, \tag{6a}$$

$$\mathcal{D}_y^k = e_{24}^k\gamma_{yz}^k + e_{25}^k\gamma_{xz}^k + \varepsilon_{12}^k\mathcal{E}_x^k + \varepsilon_{22}^k\mathcal{E}_y^k + d_{12}^k\mathcal{H}_x^k + d_{22}^k\mathcal{H}_y^k, \tag{6b}$$

$$\mathcal{D}_z^k = e_{31}^k\varepsilon_{xx}^k + e_{32}^k\varepsilon_{yy}^k + e_{33}^k\varepsilon_{zz}^k + e_{36}^k\gamma_{xy}^k + \varepsilon_{33}^k\mathcal{E}_z^k + d_{33}^k\mathcal{H}_z^k, \tag{6c}$$

$$\mathcal{B}_x^k = q_{14}^k\gamma_{yz}^k + q_{15}^k\gamma_{xz}^k + d_{11}^k\mathcal{E}_x^k + d_{12}^k\mathcal{E}_y^k + \mu_{11}^k\mathcal{H}_x^k + \mu_{12}^k\mathcal{H}_y^k, \tag{7a}$$

$$\mathcal{B}_y^k = q_{24}^k\gamma_{yz}^k + q_{25}^k\gamma_{xz}^k + d_{12}^k\mathcal{E}_x^k + d_{22}^k\mathcal{E}_y^k + \mu_{12}^k\mathcal{H}_x^k + \mu_{22}^k\mathcal{H}_y^k, \tag{7b}$$

$$\mathcal{B}_z^k = q_{31}^k\varepsilon_{xx}^k + q_{32}^k\varepsilon_{yy}^k + q_{33}^k\varepsilon_{zz}^k + q_{36}^k\gamma_{xy}^k + d_{33}^k\mathcal{E}_z^k + \mu_{33}^k\mathcal{H}_z^k, \tag{7c}$$

where C_{ij}^k are elastic coefficients, e_{ij}^k are piezoelectric coefficients, q_{ij}^k are piezomagnetic coefficients, ε_{ij}^k are electric permittivity coefficients, d_{ij}^k are electro-magnetic coupling coefficients and μ_{ij}^k are magnetic permittivity coefficients. Eqs. (2a)–(7a) allow the interaction between magnetic, electric and elastic fields.

2.3 Solution Methodology

The solution methodology for the 3D magneto-electro-elastic free vibration problem (Eq. (1a)) is here discussed in depth. The present methodology is based on a closed-form solution. Therefore, the following coefficients have to be imposed to zero:

$$C_{16}^k = C_{26}^k = C_{36}^k = C_{45}^k = 0, \quad \epsilon_{12}^k = 0, \quad \mu_{12}^k = 0, \quad d_{12}^k = 0, \tag{8}$$

$$e_{14}^k = e_{25}^k = e_{36}^k = 0, \quad q_{14}^k = q_{25}^k = q_{36}^k = 0. \tag{9}$$

The imposition suggested in Eq. (8) permits the analysis of only 0°/90° lamination angles for orthotropic laminae. The introduction of Eqs. (2a)–(4) into Eqs. (5a)–(7a) allows to write Eq. (1a) in terms

of displacements (u^k, v^k and w^k), magnetic potential ψ^k and electric potential ϕ^k. These are the primary variables of the magneto-electro-elastic free vibration problem.

Navier harmonic forms for primary variables are introduced in the planar directions of the plate as follows:

$$u^k(x,y,z,t) = U^k(z)e^{i\omega t}\cos(\bar{\alpha}x)\sin(\bar{\beta}y), \tag{10a}$$

$$v^k(x,y,z,t) = V^k(z)e^{i\omega t}\sin(\bar{\alpha}x)\cos(\bar{\beta}y), \tag{10b}$$

$$w^k(x,y,z,t) = W^k(z)e^{i\omega t}\sin(\bar{\alpha}x)\sin(\bar{\beta}y), \tag{10c}$$

$$\phi^k(x,y,z,t) = \Phi^k(z)e^{i\omega t}\sin(\bar{\alpha}x)\sin(\bar{\beta}y), \tag{10d}$$

$$\psi^k(x,y,z,t) = \Psi^k(z)e^{i\omega t}\sin(\bar{\alpha}x)\sin(\bar{\beta}y), \tag{10e}$$

where terms written in capital letters are primary variable amplitudes. $\omega = 2\pi f$ is the circular frequency, i is the imaginary unit and t indicates the time. Terms $\bar{\alpha}$ and $\bar{\beta}$ are defined as:

$$\bar{\alpha} = \frac{m\pi}{a}, \quad \bar{\beta} = \frac{n\pi}{b}, \tag{11}$$

considering a and b as the planar dimensions of flat panels and m and n the half-wave numbers in x and y directions, respectively.

Harmonic forms proposed in Eq. (10a) automatically satisfy simply supported boundary conditions for each side belonging to flat panels:

$$\begin{aligned} &v^k = 0, \quad w^k = 0, \quad \phi^k = 0, \quad \psi^k = 0, \quad \sigma^k_{xx} = 0 \quad \text{for} \quad \alpha = 0, a, \\ &u^k = 0, \quad w^k = 0, \quad \phi^k = 0, \quad \psi^k = 0, \quad \sigma^k_{yy} = 0 \quad \text{for} \quad \beta = 0, b. \end{aligned} \tag{12}$$

Navier harmonic forms allows to write the 3D set of second-order differential magneto-electro-elastic equations in terms of primary variable amplitudes and related first and second derivatives in z. The compact form of these equations is:

$$A^k_1 U^k + A^k_2 V^k + A^k_3 W^k + A^k_4 \Phi^k + A^k_5 \Psi^k + A^k_6 U^k_{,z} + A^k_7 W^k_{,z} + A^k_8 \Phi^k_{,z} + A^k_9 \Psi^k_{,z} + A^k_{10} U^k_{,zz} = 0, \tag{13a}$$

$$A^k_{11} U^k + A^k_{12} V^k + A^k_{13} W^k + A^k_{14} \Phi^k + A^k_{15} \Psi^k + A^k_{16} V^k_{,z} + A^k_{17} W^k_{,z} + A^k_{18} \Phi^k_{,z} + A^k_{19} \Psi^k_{,z} + A^k_{20} V^k_{,zz} = 0, \tag{13b}$$

$$\begin{aligned} &A^k_{21} U^k + A^k_{22} V^k + A^k_{23} W^k + A^k_{24} \Phi^k + A^k_{25} \Psi^k + A^k_{26} U^k_{,z} + A^k_{27} V^k_{,z} + A^k_{28} W^k_{,z} + A^k_{29} \Phi^k_{,z} + \\ &+ A^k_{30} \Psi^k_{,z} + A^k_{31} W^k_{,zz} + A^k_{32} \Phi^k_{,zz} + A^k_{33} \Psi^k_{,zz} = 0, \end{aligned} \tag{13c}$$

$$\begin{aligned} &A^k_{34} U^k + A^k_{35} V^k + A^k_{36} W^k + A^k_{37} \Phi^k + A^k_{38} \Psi^k + A^k_{39} U^k_{,z} + A^k_{40} V^k_{,z} + A^k_{41} W^k_{,z} + A^k_{42} W^k_{,zz} + \\ &+ A^k_{43} \Phi^k_{,zz} + A^k_{44} \Psi^k_{,zz} = 0, \end{aligned} \tag{13d}$$

$$\begin{aligned} &A^k_{45} U^k + A^k_{46} V^k + A^k_{47} W^k + A^k_{48} \Phi^k + A^k_{49} \Psi^k + A^k_{50} U^k_{,z} + A^k_{51} V^k_{,z} + A^k_{52} W^k_{,z} + A^k_{53} W^k_{,zz} + \\ &+ A^k_{54} \Phi^k_{,zz} + A^k_{55} \Psi^k_{,zz} = 0, \end{aligned} \tag{13e}$$

where each A^k_i term includes elastic coefficients, piezoelectric coefficients, magnetic coefficients and $\bar{\alpha}$ and $\bar{\beta}$ parameters.

The exponential matrix method is used as a solution in the z thickness direction. Coefficients A_i^k are constant in each k physical layer because they depend on well-known coefficients for elastic, electric and magnetic properties and on calculated terms α and β. The number of primary unknowns must be redoubled to obtain a set of first-order differential equations. This procedure has been clearly proposed in [47] where the redoubling of primary unknowns is obtained by considering in the related vector both primary variables and their first derivatives in the z thickness direction. Therefore, the final set of ten first-order differential equations in z is:

$$A_{10}^k U_{,z}^k = A_{10}^k U_{,z}^k, \tag{14a}$$

$$A_{20}^k V_{,z}^k = A_{20}^k V_{,z}^k, \tag{14b}$$

$$P_1^k W_{,z}^k = P_1^k W_{,z}^k, \tag{14c}$$

$$P_1^k \Phi_{,z}^k = P_1^k \Phi_{,z}^k, \tag{14d}$$

$$P_1^k \Psi_{,z}^k = P_1^k \Psi_{,z}^k, \tag{14e}$$

$$\begin{aligned} A_{10}^k U_{,zz}^k = &- A_1^k U^k - A_2^k V^k - A_3^k W^k - A_4^k \Phi^k - A_5^k \Psi^k - A_6^k U_{,z}^k - A_7^k W_{,z}^k + \\ &- A_8^k \Phi_{,z}^k - A_9^k \Psi_{,z}^k, \end{aligned} \tag{14f}$$

$$\begin{aligned} A_{20}^k V_{,zz}^k = &- A_{11}^k U^k - A_{12}^k V^k - A_{13}^k W^k - A_{14}^k \Phi^k - A_{15}^k \Psi^k - A_{16}^k V_{,z}^k - A_{17}^k W_{,z}^k + \\ &- A_{18}^k \Phi_{,z}^k - A_{19}^k \Psi_{,z}^k, \end{aligned} \tag{14g}$$

$$\begin{aligned} P_1^k W_{,zz}^k = &- P_2^k U^k - P_3^k V^k - P_4^k W^k - P_5^k \Phi^k - P_6^k \Psi^k - P_7^k U_{,z}^k - P_8^k V_{,z}^k - P_9^k W_{,z}^k + \\ &- P_{10}^k \Phi_{,z}^k - P_{11}^k \Psi_{,z}^k, \end{aligned} \tag{14h}$$

$$\begin{aligned} P_1^k \Phi_{,zz}^k = &- P_{12}^k U^k - P_{13}^k V^k - P_{14}^k W^k - P_{15}^k \Phi^k - P_{16}^k \Psi^k - P_{17}^k U_{,z}^k - P_{18}^k V_{,z}^k - P_{19}^k W_{,z}^k + \\ &- P_{20}^k \Phi_{,z}^k - P_{21}^k \Psi_{,z}^k, \end{aligned} \tag{14i}$$

$$\begin{aligned} P_1^k \Psi_{,zz}^k = &- P_{22}^k U^k - P_{23}^k V^k - P_{24}^k W^k - P_{25}^k \Phi^k - P_{26}^k \Psi^k - P_{27}^k U_{,z}^k - P_{28}^k V_{,z}^k - P_{29}^k W_{,z}^k + \\ &- P_{30}^k \Phi_{,z}^k - P_{31}^k \Psi_{,z}^k. \end{aligned} \tag{14j}$$

Eq. (14a) are solved via the exponential matrix method. Coefficients P_i^k are explicitly given in the Appendix A section.

Matrix form of Eq. (14a) is:

$$\boldsymbol{D}^k \boldsymbol{X}_{,z}^k = \boldsymbol{A}^k \boldsymbol{X}^k \Rightarrow \boldsymbol{X}_{,z}^k = \boldsymbol{A}^{*j} \boldsymbol{X}^k, \tag{15}$$

where $\boldsymbol{X}^k$ and $\boldsymbol{X}_{,z}^k$ primary variable amplitudes and related derivatives in z, respectively. The 10×1 vector is $\boldsymbol{X}^k = \{U(z)^k, V(z)^k, W(z)^k, \Phi(z)^k, \Psi(z)^k, U(z)_{,z}^k, V(z)_{,z}^k, W(z)_{,z}^k, \Phi(z)_{,z}^k, \Psi(z)_{,z}^k\}$. The solution of Eq. (15) is obtained by applying the exponential matrix method via the Taylor expansion [47]:

$$\boldsymbol{X}^k(h_k) = \boldsymbol{A}^{**k} \boldsymbol{X}^k(0) = \left[\sum_{i=0}^{N} \frac{(\boldsymbol{A}^{*k})^i}{i!} h_k^i \right] \boldsymbol{X}^k(0). \tag{16}$$

where $(\boldsymbol{A}^{*k})^0 = \boldsymbol{I}$ is the 10×10 identity matrix. k indicates the layer and it goes from 1 (first layer) to M (last layer). h_k is the layer thickness for each physical layer.

Interlaminar continuity conditions for primary variables, transverse normal and transverse shear stresses (σ_{zz}^k, σ_{xz}^k, σ_{yz}^k), transverse normal electric displacement component ($\mathcal{D}_z^k$) and transverse normal magnetic induction component ($\mathcal{B}_z^k$) are fundamental to obtain a layer wise model. Interlaminar continuity conditions consider the top (t) of the $k-1$ layer and the bottom (b) of the k layer.

Interlaminar continuity conditions are imposed as:

$$u_b^k = u_t^{k-1}, \quad v_b^k = v_t^{k-1}, \quad w_b^k = w_t^{k-1}, \quad \phi_b^k = \phi_t^{k-1}, \quad \psi_b^k = \psi_t^{k-1} \tag{17a}$$

$$\sigma_{xz_b}^k = \sigma_{xz_t}^{k-1}, \quad \sigma_{yz_b}^k = \sigma_{yz_t}^{k-1}, \quad \sigma_{zz_b}^k = \sigma_{zz_t}^{k-1}, \quad \mathcal{D}_{z_b}^k = \mathcal{D}_{z_t}^{k-1}, \quad \mathcal{B}_{z_b}^k = \mathcal{B}_{z_t}^{k-1}. \tag{17b}$$

The introduction of Eqs. (5a)–(7a) and (10a) in Eq. (17) allows interlaminar continuity conditions written in terms of maximum amplitudes:

$$U_b^k = U_t^{k-1}, \tag{18a}$$

$$V_b^k = V_t^{k-1}, \tag{18b}$$

$$W_b^k = W_t^{k-1}, \tag{18c}$$

$$\Phi_b^k = \Phi_t^{k-1}, \tag{18d}$$

$$\Psi_b^k = \Psi_t^{k-1}, \tag{18e}$$

$$C_{55}^k \bar{\alpha} W_b^k + C_{55}^k U_{,z_b}^k + e_{15}^k \bar{\alpha} \Phi_b^k + q_{15}^k \bar{\alpha} \Psi_b^k = C_{55}^{k-1} \bar{\alpha} W_t^{k-1} + C_{55}^{k-1} U_{,z_t}^{k-1} + e_{15}^{k-1} \bar{\alpha} \Phi_t^{k-1} + q_{15}^{k-1} \bar{\alpha} \Psi_t^{k-1}, \tag{18f}$$

$$C_{44}^k \bar{\beta} W_b^k + C_{44}^k V_{,z_b}^k + e_{24}^k \bar{\beta} \Phi_b^k + q_{24}^k \bar{\beta} \Psi_b^k = C_{44}^{k-1} \bar{\beta} W_t^{k-1} + C_{44}^{k-1} V_{,z_t}^{k-1} + e_{25}^{k-1} \bar{\beta} \Phi_t^{k-1} + q_{25}^{k-1} \bar{\beta} \Psi_t^{k-1}, \tag{18g}$$

$$\begin{aligned} &C_{13}^k \bar{\alpha} U_b^k - C_{23}^k \bar{\beta} V_b^k + C_{33}^k W_{,z_b}^k + e_{33}^k \Phi_{,z_b}^k + q_{33}^k \Psi_{,z_b}^k = -C_{13}^{k-1} \bar{\alpha} U_t^{k-1} - C_{23}^{k-1} \bar{\beta} V_t^{k-1} + C_{33}^{k-1} W_{,z_t}^{k-1} + \\ &+ e_{33}^{k-1} \Phi_{,z_t}^{k-1} + q_{33}^{k-1} \Psi_{,z_t}^{k-1}, \end{aligned} \tag{18h}$$

$$\begin{aligned} &- e_{31}^k \bar{\alpha} U_b^k - e_{32}^k \bar{\beta} V_b^k + e_{33}^k W_{,z_b}^k - \varepsilon_{33}^k \Phi_{,z_b}^k - d_{33}^k \Psi_{,z_b}^k = -e_{31}^{k-1} \bar{\alpha} U_t^k - e_{32}^{k-1} \bar{\beta} V_t^k + e_{33}^{k-1} W_{,z_t}^{k-1} + \\ &- \varepsilon_{33}^{k-1} \Phi_{,z_t}^{k-1} - d_{33}^{k-1} \Psi_{,z_t}^{k-1}, \end{aligned} \tag{18i}$$

$$\begin{aligned} &- q_{31}^k \bar{\alpha} U_b^k - q_{32}^k \bar{\beta} V_b^k + q_{33}^k W_{,z_b}^k - d_{33}^k \Phi_{,z_b}^k - \mu_{33}^k \Psi_{,z_b}^k = -q_{31}^{k-1} \bar{\alpha} U_t^k - q_{32}^{k-1} \bar{\beta} V_t^k + q_{33}^{k-1} W_{,z_t}^{k-1} + \\ &- d_{33}^{k-1} \Phi_{,z_t}^{k-1} - \mu_{33}^{k-1} \Phi_{,z_t}^{k-1}. \end{aligned} \tag{18j}$$

The matrix form is:

$$\boldsymbol{X}_b^k = \boldsymbol{T}^{k,k-1} \boldsymbol{X}_t^{k-1}, \tag{19}$$

where $\boldsymbol{T}^{k,k-1}$ is the 10×10 transfer, it allows to link interfaces between two adjacent layers k and $k-1$. In Eq. (19), $\boldsymbol{X}_t^k$ means $\boldsymbol{X}^k(h_k)$ and $\boldsymbol{X}_b^k$ means $\boldsymbol{X}^k(0)$.

The recursive introduction of Eq. (16) in Eq. (19) allows the solution along the z thickness direction. The final equation has the following form:

$$\boldsymbol{X}_t^M = \boldsymbol{H_m} \boldsymbol{X}_b^1, \tag{20}$$

where $\boldsymbol{H_m} = \boldsymbol{A}^{**M} \boldsymbol{T}^{M,M-1} \ldots \boldsymbol{T}^{2,1} \boldsymbol{A}^{**1}$. Matrix $\boldsymbol{H_m}$ includes the matrices $\boldsymbol{T}^{k,k-1}$ and $\boldsymbol{A}^{**k}$ computed for each k layer of the multilayered plate. M is the last layer at the top and 1 is the first layer at the bottom. These

two matrices include elastic, magnetic and electric material coefficients, dimensions for the flat panel and thickness of each layer. The most important feature of matrix $\boldsymbol{H_m}$ is the 10×10 dimension, independently of the number of k layers involved in the multilayered configuration and the order N used in Eq. (16). In this way, a low computational cost is guaranteed.

Load boundary conditions for open-circuit and closed-circuit configurations are:

$$\sigma_{zz} = 0, \quad \sigma_{xz} = 0, \quad \sigma_{yz} = 0, \quad \mathcal{D}_z = 0, \quad \mathcal{B}_z = 0 \quad \text{for} \quad z = \pm h/2 \quad \text{(open circuit)} \tag{21}$$

$$\sigma_{zz} = 0, \quad \sigma_{xz} = 0, \quad \sigma_{yz} = 0, \quad \phi = 0, \quad \psi = 0 \quad \text{for} \quad z = \pm h/2 \quad \text{(closed circuit)}. \tag{22}$$

The open-circuit configuration may be explicitly stated as:

$$\sigma^1_{zz_b} = -C^1_{13}\bar{\alpha}U^1_b - C^1_{23}\bar{\beta}V^1_b + C^1_{33}W^1_{,z_b} + e^1_{33}\Phi^1_{,z_b} + q^1_{33}\Psi^1_{,z_b} = 0, \tag{23a}$$

$$\sigma^1_{yz_b} = C^1_{44}\bar{\beta}W^1_b + C^1_{44}V^1_{,z_b} + e^1_{24}\bar{\beta}\Phi^1_b + q^1_{24}\bar{\beta}\Psi^1_b = 0, \tag{23b}$$

$$\sigma^1_{xz_b} = C^1_{55}\bar{\alpha}W^1_b + C^1_{55}U^1_{,z_b} + e^1_{15}\bar{\alpha}\Phi^1_b + q^1_{15}\bar{\alpha}\Psi^1_b = 0, \tag{23c}$$

$$\mathcal{D}^1_{z_b} = e^1_{31}\bar{\alpha}U^1_b + e^1_{32}\bar{\beta}V^1_b + e^1_{33}W^1_{,z_b} - \varepsilon^1_{33}\Phi^1_{,z_b} - d^1_{33}\Psi^1_{,z_b} = 0, \tag{23d}$$

$$\mathcal{B}^1_{z_b} = q^1_{31}\bar{\alpha}U^1_b + q^1_{32}\bar{\beta}V^1_b + q^1_{33}W^1_{,z_b} - d^1_{33}\Phi^1_{,z_b} - \mu^1_{33}\Psi^1_{,z_b} = 0, \tag{23e}$$

$$\sigma^M_{zz_t} = -C^M_{13}\bar{\alpha}U^M_t - C^M_{23}\bar{\beta}V^M_t + C^M_{33}W^M_{,z_t} + e^M_{33}\Phi^M_{,z_t} + q^M_{33}\Psi^M_{,z_t} = 0, \tag{23f}$$

$$\sigma^M_{\beta z_t} = C^M_{44}\bar{\beta}W^M_t + C^M_{44}V^M_{,z_t} + e^M_{24}\bar{\beta}\Phi^M_t + q^M_{24}\bar{\beta}\Psi^M_t = 0, \tag{23g}$$

$$\sigma^M_{\alpha z_t} = C^M_{55}\bar{\alpha}W^M_t + C^M_{55}U^M_{,z_t} + e^M_{15}\bar{\alpha}\Phi^M_t + q^M_{15}\bar{\alpha}\Psi^M_t = 0, \tag{23h}$$

$$\mathcal{D}^M_{z_t} = e^M_{31}\bar{\alpha}U^M_t + e^M_{32}\bar{\beta}V^M_t + e^M_{33}W^M_{,z_t} - \varepsilon^M_{33}\Phi^M_{,z_t} - d^M_{33}\Psi^M_{,z_t} = 0, \tag{23i}$$

$$\mathcal{B}^M_{z_t} = q^M_{31}\bar{\alpha}U^M_t + q^M_{32}\bar{\beta}V^M_t + q^M_{33}W^M_{,z_t} - d^M_{33}\Phi^M_{,z_t} - \mu^M_{33}\Psi^M_{,z_t} = 0. \tag{23j}$$

The closed-circuit configuration can be explicity written as:

$$\sigma^1_{zz_b} = -C^1_{13}\bar{\alpha}U^1_b - C^1_{23}\bar{\beta}V^1_b + C^1_{33}W^1_{,z_b} + e^1_{33}\Phi^1_{,z_b} + q^1_{33}\Psi^1_{,z_b} = 0, \tag{24a}$$

$$\sigma^1_{\beta z_b} = C^1_{44}\bar{\beta}W^1_b + C^1_{44}V^1_{,z_b} + e^1_{24}\bar{\beta}\Phi^1_b + q^1_{24}\bar{\beta}\Psi^1_b = 0, \tag{24b}$$

$$\sigma^1_{\alpha z_b} = C^1_{55}\bar{\alpha}W^1_b + C^1_{55}U^1_{,z_b} + e^1_{15}\bar{\alpha}\Phi^1_b + q^1_{15}\bar{\alpha}\Psi^1_b = 0, \tag{24c}$$

$$\Phi^1_b = 0, \tag{24d}$$

$$\Psi^1_b = 0, \tag{24e}$$

$$\sigma^M_{zz_t} = -C^M_{13}\bar{\alpha}U^M_t - C^M_{23}\bar{\beta}V^M_t + C^M_{33}W^M_{,z_t} + e^M_{33}\Phi^M_{,z_t} + q^M_{33}\Psi^M_{,z_t} = 0, \tag{24f}$$

$$\sigma^M_{\beta z_t} = C^M_{44}\bar{\beta}W^M_t + C^M_{44}V^M_{,z_t} + e^M_{24}\bar{\beta}\Phi^M_t + q^M_{24}\bar{\beta}\Psi^M_t = 0, \tag{24g}$$

$$\sigma^M_{\alpha z_t} = C^M_{55}\bar{\alpha}W^M_t + C^M_{55}U^M_{,z_t} + e^M_{15}\bar{\alpha}\Phi^M_t + q^M_{15}\bar{\alpha}\Psi^M_t = 0. \tag{24h}$$

$$\Phi^M_t = 0, \tag{24i}$$

$$\Psi^M_t = 0. \tag{24j}$$

Both open and closed circuit conditions can be further compacted in matrix form as:

$$\boldsymbol{B}_b^1 \boldsymbol{X}_b^1 = \boldsymbol{0}, \tag{25a}$$

$$\boldsymbol{B}_t^M \boldsymbol{X}_t^M = \boldsymbol{0}, \tag{25b}$$

where $\boldsymbol{B}_b^1$ and $\boldsymbol{B}_t^M$ are the generic 5×10 load boundary condition matrices at the bottom (b) of the first layer (1) and at top (t) of the last layer (M), respectively. Eq. (25) can be rewritten by using Eq. (20):

$$\begin{bmatrix} \boldsymbol{B}_t^M \boldsymbol{H_m} \\ \boldsymbol{B}_b^1 \end{bmatrix} \boldsymbol{X}_b^1 = \begin{Bmatrix} \boldsymbol{0} \\ \boldsymbol{0} \end{Bmatrix} \Rightarrow \boldsymbol{E} \boldsymbol{X}_b^1 = \boldsymbol{0}. \tag{26}$$

The null space of matrix $\boldsymbol{E}$ must be imposed via the computation of eigenvalues. The determinant allows to compute eigenvalues and eigenvectors. Matrix $\boldsymbol{E}$ determinant is a polynomial function in terms of ω^2, where $\omega = 2\pi f$ is the circular frequency. Solving the equation, the minor ω value satisfying the polynomial equation makes null the space of matrix $\boldsymbol{E}$. Therefore, the eigenvectors and eigenvalues computation of matrix $\boldsymbol{E}$ by considering the proper ω^2 value is possible. Eigenvectors can be evaluated along the thickness direction of the flat panel via the recursive use of Eqs. (16) and (19). In this way, frequency modes along the thickness direction are shown considering displacements, magnetic potential, electric potential, transverse normal magnetic induction/electric displacement and stresses.

3 Results

The results section is made up of two subsections. In the first one, two assessment cases are shown to validate the present 3D coupled magneto-electro-elastic model (called 3D-u-ϕ-ψ). Comparisons are made using a 3D electro-elastic model (3D-u-ϕ) and a 3D magneto-elastic model (3D-u-ψ). Then, a new multilayered plate case is studied considering different thickness ratios.

The 3D-u-ϕ-ψ model is preliminarily confronted with the 3D-u-ϕ model by Brischetto and Cesare [43] and with the 3D-u-ψ model by Brischetto and Cesare [44]. Open-circuit and closed-circuit configurations are validated. For both assessments, different a/h ratios are compared. A complete validation is proposed because magnetic and electric fields are separately validated considering thick and thin flat panels. Further effects involved in the flat panels, such as material and thickness layer effects, are evaluated. Comparisons are proposed in terms of the first three circular frequency values $\bar{\omega}$ for several (m, n). Third and fourth assessments also verify the full electro-elastic-magnetic coupling correctness.

In the benchmark subsection, a multilayered square flat panel is analyzed under open-circuit and closed-circuit conditions. The first five circular frequencies $\bar{\omega}$ for different (m, n) couples are reported in tabular form. First three frequency modes through the z direction are represented in graphical form for different thickness ratios a/h. These frequency modes are given considering normalized displacements u^*, v^* and w^*, electric potential ϕ^*, magnetic potential ψ^*, transverse normal stress σ_{zz}^*, transverse normal electric displacement $\mathcal{D}_z^*$ and transverse normal magnetic induction $\mathcal{B}_z^*$. Normalization for each variable is performed by dividing each variable by its maximum value.

3.1 Assessments

In the first two proposed assessments, the magnetic permittivity coefficients μ_1 and μ_2 for the $CoFe_2O_4$ are considered equal to $-590 \cdot 10^3$ nH/m in Table 1 to be coherent with reference results proposed in [43] and [44]. Elastic material properties in terms of Young modulus (E_i), shear modulus (G_{ij}) and Poisson ratio (ν_{ij}) have been computed from C_{ij} elastic coefficients by considering relations proposed in [48].

Table 1: Elastic, electric and magnetic material data for structures analyzed in assessments and benchmarks

	PZT-4 [43]	**Al2024** [43,44]	**PVDF** [43,44]	$CoFe_2O_4$ [44]	**Foam** [44]	$BaTiO_3$ [49]	**Adaptive wood** [1,50]	**Composite** [44]
E_1 [GPa]	81.3	73	237	154.32	0.180	116.33	154.32	172.37
E_2 [GPa]	81.3	73	23.2	154.32	0.180	116.33	154.32	6.895
E_3 [GPa]	64.5	73	10.5	142.83	0.180	111.93	142.83	6.895
ν_{12}	0.329	0.3	0.154	0.36564	0.37	0.30709	0.36564	0.25
ν_{13}	0.432	0.3	0.178	0.40133	0.37	0.33362	0.40133	0.25
ν_{23}	0.432	0.3	0.177	0.40133	0.37	0.33362	0.40133	0.25
G_{12} [GPa]	30.6	28.077	6.43	56.5	0.065693	44.5	56.5	3.447
G_{13} [GPa]	25.6	28.077	4.40	45.3	0.065693	43	45.3	3.447
G_{23} [GPa]	25.6	28.077	2.15	45.3	0.065693	43	45.3	1.379
e_{15} [C/m^2]	12.72	0	−0.01	0	0	11.6	11.6	0
e_{24} [C/m^2]	12.72	0	−0.01	0	0	11.6	11.6	0
e_{31} [C/m^2]	−5.20	0	−0.13	0	0	−4.4	−4.4	0
e_{32} [C/m^2]	−5.20	0	−0.14	0	0	−4.4	−4.4	0
e_{33} [C/m^2]	15.08	0	−0.28	0	0	18.6	18.6	0
ε_1 [nF/m]	0.008854	0.008854	0.1107	0.08	0.008854	11.2	0.08	0.008854
ε_2 [nF/m]	0.008854	0.008854	0.1061	0.08	0.008854	11.2	0.08	0.008854
ε_3 [nF/m]	0.008854	0.008854	0.1061	0.093	0.008854	12.6	0.093	0.008854
q_{15} [T]	0	0	0	550	0	0	560	0
q_{24} [T]	0	0	0	550	0	0	560	0
q_{31} [T]	0	0	0	580.3	0	0	580	0
q_{32} [T]	0	0	0	580.3	0	0	580	0
q_{33} [T]	0	0	0	699.7	0	0	700	0
μ_1 [nH/m]	$4\pi \cdot 10^2$	$4\pi \cdot 10^2$	$4\pi \cdot 10^2$	$-590 \cdot 10^3$	$4\pi \cdot 10^2$	$5 \cdot 10^3$	$590 \cdot 10^3$	$4\pi \cdot 10^2$
μ_2 [nH/m]	$4\pi \cdot 10^2$	$4\pi \cdot 10^2$	$4\pi \cdot 10^2$	$-590 \cdot 10^3$	$4\pi \cdot 10^2$	$5 \cdot 10^3$	$590 \cdot 10^3$	$4\pi \cdot 10^2$
μ_3 [nH/m]	$4\pi \cdot 10^2$	$4\pi \cdot 10^2$	$4\pi \cdot 10^2$	$157 \cdot 10^3$	$4\pi \cdot 10^2$	$10 \cdot 10^3$	$157 \cdot 10^3$	$4\pi \cdot 10^2$
d_1 [Ns/VC]	0	0	0	0	0	0	$3 \cdot 10^{-12}$	0
d_2 [Ns/VC]	0	0	0	0	0	0	$3 \cdot 10^{-12}$	0
d_3 [Ns/VC]	0	0	0	0	0	0	$3 \cdot 10^{-12}$	0
ρ [kg/m^3]	7600	2800	1800	variable	50	1	5300	1500

The first assessment (A1) considers a simply supported multilayered square flat panel with in-plane dimensions $a = b = 1$ m and variable thickness h. Multilayered configuration is PZT-4/Al2024/PVDF/Al2024/PZT-4 where $h_{PZT-4} = h_{Al2024} = 0.1h$ and $h_{PVDF} = 0.6h$. h is the total thickness of the flat panel. Both closed circuit (A1-CC) and open circuit (A1-OC) configurations are validated. The open circuit configuration for the electro-elastic case states $\mathcal{D}_{z_t} = \mathcal{D}_{z_b} = 0$ C/m^2; the closed circuit configuration imposes $\phi_t = \phi_b = 0$ V. Three different impositions for half-wave number couples are analyzed for open and closed circuit configurations: $m = n = 1$, $m = 1$ and $n = 2$ and $m = n = 2$. The first three frequencies are given for each (m,n) couple. Properties related to mechanical, electric and magnetic material coefficients are reported in Table 1. Comparisons are performed considering as reference solution the 3D-u-ϕ electro-elastic model by Brischetto and Cesare [43]. In Tables 2 and 3, the first three circular frequencies $\bar{\omega}$ for several (m, n) values are compared with the reference solution for thick $(a/h = 4)$, moderately thick $(a/h = 10, 20)$ and thin $(a/h = 50, 100)$ flat panels in both closed-circuit and open-circuit configurations. A perfect matching is shown when the 3D-u-ϕ-ψ electro-magneto-elastic model is confronted with the 3D-u-ϕ model for each thickness ratio. Results in Tables 2 and 3 allow to state that the 3D-u-ϕ-ψ model opportunely includes the electro-elastic coupling, and related material and thickness layer effects. Differences between results obtained in closed circuit configuration and results obtained in open circuit configuration are very small. These small differences are more evident for thicker plates and higher (m,n) values.

Table 2: Assessment A1-CC, layered electro-elastic square flat panel in closed circuit configuration. Free vibration analysis for simply supported sides

	a/h	4	10	20	50	100
			$\bar{\omega} = \omega/100$			
(1,1)-I	3D-u-ϕ [43]	39.165	25.172	14.499	6.0930	3.0695
	3D-u-ϕ-ψ	39.165	25.172	14.499	6.0930	3.0695
(1,1)-II	3D-u-ϕ [43]	131.62	135.66	136.30	136.49	136.52
	3D-u-ϕ-ψ	131.62	135.66	136.30	136.49	136.52
(1,1)-III	3D-u-ϕ [43]	163.96	247.27	250.72	251.72	251.86
	3D-u-ϕ-ψ	163.96	247.27	250.72	251.72	251.86
			$\bar{\omega} = \omega/100$			
(1,2)-I	3D-u-ϕ [43]	64.895	48.306	31.569	14.197	7.2389
	3D-u-ϕ-ψ	64.895	48.306	31.569	14.197	7.2389
(1,2)-II	3D-u-ϕ [43]	204.89	225.81	228.02	228.65	228.75
	3D-u-ϕ-ψ	204.88	225.81	228.02	228.65	228.74
(1,2)-III	3D-u-ϕ [43]	224.53	301.55	303.75	304.32	304.40
	3D-u-ϕ-ψ	224.52	301.55	303.75	304.32	304.40
			$\bar{\omega} = \omega/100$			
(2,2)-I	3D-u-ϕ [43]	93.894	72.517	50.344	23.679	12.186
	3D-u-ϕ-ψ	93.893	72.517	50.344	23.679	12.186
(2,2)-II	3D-u-ϕ [43]	215.21	266.56	271.31	272.77	272.98
	3D-u-ϕ-ψ	215.19	266.56	271.31	272.77	272.98
(2,2)-III	3D-u-ϕ [43]	263.76	362.11	494.54	502.30	503.44
	3D-u-ϕ-ψ	263.75	362.11	494.54	502.29	503.44

Table 3: Assessment A1-OC, layered electro-elastic square falt panel in open circuit configuration. Free vibration analysis for simply supported sides

	a/h	4	10	20	50	100
		$\bar{\omega} = \omega/100$				
(1,1)-I	3D-u-ϕ [43]	39.172	25.173	14.500	6.0930	3.0695
	3D-u-ϕ-ψ	39.172	25.173	14.500	6.0930	3.0695
(1,1)-II	3D-u-ϕ [43]	131.62	135.66	136.31	136.49	136.52
	3D-u-ϕ-ψ	131.62	135.66	136.31	136.50	136.53
(1,1)-III	3D-u-ϕ [43]	163.97	247.32	250.74	251.73	251.88
	3D-u-ϕ-ψ	163.97	247.32	250.74	251.73	251.88
		$\bar{\omega} = \omega/100$				
(1,2)-I	3D-u-ϕ [43]	64.922	48.310	31.570	14.197	7.2389
	3D-u-ϕ-ψ	64.922	48.310	31.570	14.197	7.2389
(1,2)-II	3D-u-ϕ [43]	204.89	225.81	228.02	228.66	228.75
	3D-u-ϕ-ψ	204.88	225.81	228.02	228.66	228.75
(1,2)-III	3D-u-ϕ [43]	224.54	301.60	303.78	304.35	304.43
	3D-u-ϕ-ψ	224.52	301.60	303.78	304.35	304.43
		$\bar{\omega} = \omega/100$				
(2,2)-I	3D-u-ϕ [43]	93.954	72.525	50.346	23.679	12.186
	3D-u-ϕ-ψ	93.954	72.525	50.346	23.679	12.186
(2,2)-II	3D-u-ϕ [43]	215.21	266.56	271.32	272.78	273.00
	3D-u-ϕ-ψ	215.19	266.56	271.32	272.78	273.00
(2,2)-III	3D-u-ϕ [43]	263.76	362.13	494.63	502.33	503.47
	3D-u-ϕ-ψ	263.75	362.13	494.63	502.33	503.47

In the second assessment (A2), a simply supported multilayered square flat panel is considered. In-plane dimensions are $a = b = 1\ m$ and the thickness h is variable. The multilayered configuration is $CoFe_2O_4$/Al2024/Foam/Al2024/$CoFe_2O_4$ where $h_{CoFe_2O_4} = h_{Al2024} = 0.1h$ and $h_{PVDF} = 0.6h$; h is the total thickness of the multilayered flat panel. Material mass density of the $CoFe_20_4$ for this assessment is $\rho_{CoFe_20_4} = 5300\ \text{kg/m}^3$. The open-circuit configuration (OC) is analyzed. This configuration states $\mathcal{B}_{z_t} = \mathcal{B}_{z_b} = 0\ T$. Material properties in terms of elastic, electric and magnetic coefficients are reported in Table 1. The reference solution used is the 3D-u-ψ magneto-elastic model in [44]. In Table 4, the first three circular frequencies $\bar{\omega}$ for (1,1), (2,2) and (3,3) half-wave couples are reported for the same thickness ratios proposed in A1. Even in this case, a perfect matching is highlighted between $\bar{\omega}$ values computed with the 3D-u-ϕ-ψ electro-magneto-elastic model and those calculated with the 3D-u-ψ magneto-elastic model. This feature is confirmed for each thickness ratio. Results presented in Table 4 permit validation of the magneto-elastic coupling and related material and thickness layer effects for thick, moderately thick and thin multilayered magneto-elastic flat panels.

Table 4: Assessment A2-OC, layered magneto-elastic square flat panel in open circuit configuration. Free vibration analysis for simply supported sides

	a/h	4	10	20	50	100
		ω				
(1,1)-I	3D-u-ψ [44]	0.0558	0.0352	0.0296	0.0214	0.0133
	3D-u-ϕ-ψ	0.0558	0.0352	0.0296	0.0214	0.0133
(1,1)-II	3D-u-ψ [44]	0.1420	0.3559	0.4503	0.4504	0.4504
	3D-u-ϕ-ψ	0.1420	0.3559	0.4503	0.4504	0.4504
(1,1)-III	3D-u-ψ [44]	0.4491	0.4502	0.5589	0.7871	0.7873
	3D-u-ϕ-ψ	0.4491	0.4502	0.5589	0.7871	0.7873
		ω				
(2,2)-I	3D-u-ψ [44]	0.1928	0.0965	0.0704	0.0559	0.0428
	3D-u-ϕ-ψ	0.1928	0.0965	0.0704	0.0559	0.0428
(2,2)-II	3D-u-ψ [44]	0.2190	0.3510	0.7117	0.9007	0.9007
	3D-u-ϕ-ψ	0.2190	0.3510	0.7117	0.9007	0.9007
(2,2)-III	3D-u-ψ [44]	0.8072	0.8993	0.9004	1.2212	1.5742
	3D-u-ϕ-ψ	0.8072	0.8993	0.9004	1.2212	1.5742
		ω				
(3,3)-I	3D-u-ψ [44]	0.4062	0.1913	0.1239	0.0925	0.0768
	3D-u-ϕ-ψ	0.4062	0.1913	0.1239	0.0925	0.0768
(3,3)-II	3D-u-ψ [44]	0.4137	0.3676	0.7049	1.3510	1.3511
	3D-u-ϕ-ψ	0.4137	0.3676	0.7049	1.3510	1.3511
(3,3)-III	3D-u-ψ [44]	0.8968	1.3443	1.3500	1.5863	2.1284
	3D-u-ϕ-ψ	0.8968	1.3443	1.3500	1.5863	2.1284

In the assessment number three (A3), a simply supported three-layered thick square flat panel is considered. Geometrical dimensions are $a = b = h = 0.3$ m. (m, n) half-wave couples equal to (1,1) have been used. The lamination stacking sequence is $BaTiO_3/CoFe_2O_4/BaTiO_3$ where each lamina is 0.1 m thick. Material mass density of the $CoFe_20_4$ is $\rho_{CoFe_20_4} = 1\,\text{kg/m}^3$ as stated in [49]. Both open circuit ($\mathcal{D}_{z_t} = \mathcal{D}_{z_b} = 0\ \text{C/m}^2$ and $\mathcal{B}_{z_t} = \mathcal{B}_{z_b} = 0\ \text{C/m}^2$) and closed circuit ($\phi_t = \phi_b = 0$ V and $\psi_t = \psi_b = 0$ V) configurations have been analyzed. Elastic, electric and magnetic material properties for $BaTiO_3$ and $CoFe_2O_4$ are included in Table 1. Reference solution is the manuscript by Chen et al. [49] related to the 3D free vibration analysis of magneto-electro-elastic model for plates. In Table 5, the first seven no-dimensional circular frequencies in both open circuit and closed circuit configuration are compared with the 3D-u-ϕ-ψ model. These calculated values are in agreement with the 3D reference solution by Chen et al. [49]. This validation permits the correct depiction of all the effects involved in thick square flat panels (thickness layer and material layer effects) by considering the full magneto-electro-elastic coupling.

In the fourth assessment (A4), a simply supported three-layered thick square flat panel is presented considering both open and closed circuit cases. Geometrical dimensions, half-wave couples (m, n) and material mass density for $CoFe_2O_4$ are the same as seen in the A3 case. The multilayered configuration scheme is $CoFe_2O_4/BaTiO_3/CoFe_2O_4$ considering each lamina 0.1 m thick. Material properties of the two laminae involved in this assessment are written in Table 1. The benchmark solution is the paper by Chen et al. [49]. Table 6 shows the first seven non-dimensional circular frequencies for the multilayered flat panel.

It is possible to see a very good accordance with the 3D benchmark solution [49] for both load boundary conditions. This feature is confirmed for each investigated non-dimensional circular frequency. This validation attests that the proposed model correctly includes all involved effects for magneto-electro-elastic flat panels.

Table 5: Assessment A3, layered magneto-electro-elastic square flat panel $BaTiO_3/CoFe_2O_4/BaTiO_3$ in open circuit and closed circuit configuration. Free vibration analysis for simply supported sides. C_{max} = 286 GPa and ρ_{max} = 1 kg/m^3 are the maximum elastic coefficients and the maximum mass density of the proposed structure

		Open circuit	Closed circuit
		$\bar{\omega} = \omega a\sqrt{\rho_{max}/C_{max}}$	
(1,1)-I	3D [49]	1.5474	1.5337
	3D-u-ϕ-ψ	1.5474	1.5336
(1,1)-II	3D [49]	1.8265	1.8265
	3D-u-ϕ-ψ	1.8247	1.8247
(1,1)-III	3D [49]	2.1556	2.1556
	3D-u-ϕ-ψ	2.1556	2.1556
(1,1)-IV	3D [49]	2.2448	2.2333
	3D-u-ϕ-ψ	2.2448	2.2330
(1,1)-V	3D [49]	3.0765	3.0222
	3D-u-ϕ-ψ	3.0764	3.0222
(1,1)-VI	3D [49]	3.0834	3.0765
	3D-u-ϕ-ψ	3.0834	3.0765
(1,1)-VII	3D [49]	3.4438	3.3452
	3D-u-ϕ-ψ	3.4437	3.3452

Table 6: Assessment A4, layered magneto-electro-elastic square flat panel $CoFe_2O_4/BaTiO_3/CoFe_2O_4$ in open circuit and closed circuit configuration. Free vibration analysis for simply supported sides. C_{max} = 286 GPa and ρ_{max} = 1 kg/m^3 are the maximum elastic coefficients and the maximum mass density of the proposed structure

		Open circuit	Closed circuit
		$\bar{\omega} = \omega a\sqrt{\rho_{max}/C_{max}}$	
(1,1)-I	3D [49]	1.6054	1.6052
	3D-u-ϕ-ψ	1.6054	1.6039
(1,1)-II	3D [49]	1.8987	1.8987
	3D-u-ϕ-ψ	1.8986	1.8986
(1,1)-III	3D [49]	2.2475	2.2474
	3D-u-ϕ-ψ	2.2475	2.2465
(1,1)-IV	3D [49]	2.3156	2.3156
	3D-u-ϕ-ψ	2.3156	2.3156
(1,1)-V	3D [49]	3.1156	3.1156
	3D-u-ϕ-ψ	3.1156	3.1156
(1,1)-VI	3D [49]	3.2216	3.2215
	3D-u-ϕ-ψ	3.2216	3.2215
(1,1)-VII	3D [49]	3.7369	3.7369
	3D-u-ϕ-ψ	3.7371	3.7451

The results proposed in all these assessments have been obtained with an order $N = 7$ for the exponential matrix. This order has been obtained after a convergence analysis and it gives proper results for the various thickness ratio, (m, n) couple and frequency order. For this reason, it will also be employed in the benchmark subsection. This assessment section stated the correctness of the mathematical formulation and the effectiveness of the implementation of the 3D-u-ϕ-ψ model. Thanks to the first two assessments (A1 and A2), electro-elastic and magneto-elastic couplings have been separately assessed. This procedure permits stating that the present 3D-u-ϕ-ψ model correctly decouples the electro-elastic effect and the magneto-elastic effect. Then, the other two assessments (A3 and A4) include the full magneto-electro-elastic coupling. Even for these assessments, the proposed 3D-u-ϕ-ψ model correctly depicts all the involved effects for a magneto-electro-elastic multilayered flat panel. Therefore, all possible configurations have been tested and it is possible to state that a very good robustness and correct depiction of all involved effects are shown in the case of the free vibration analysis of a magneto-electro-elastic multilayered flat panel (magneto-electro-elastic coupling, thickness layer effect and material layer effect). For this reason, the 3D-u-ϕ-ψ model can be used in the following subsection to present new multilayered flat panel cases involving magneto-electro-elastic effects.

3.2 Benchmarks

In this benchmark subsection, the magnetic permittivity coefficients μ_1 and μ_2 for the Adaptive Wood are equal to $+590 \cdot 10^3$ nH/m in Table 1 for physical reasons as discussed in Pan [50]. The minus sign was considered in the assessment subsection to allow for comparison with results already obtained in the literature. For these new results, we prefer to be physically consistent.

The proposed benchmark considers a multilayered square flat panel embedding external skins made of Adaptive wood and an internal composite laminated core with stacking sequence /0°/90°/0°. The thickness of each external skin is $h_{Adaptive\ wood} = 0.05h$, the thickness of each internal composite lamina is $h_{Composite} = 0.3h$. h is the global thickness of the flat panel. The plate dimensions are $a = b = 1$ m. First five circular frequencies $\bar{\omega}$ are proposed for both closed circuit (CC) and open circuit (OC) configurations. Imposed half-wave numbers (m, m) for each case are (1,1), (1,2), (2,1), (2,2), (3,1) and (3,2). $\mathcal{D}_{z_t} = \mathcal{D}_{z_b} = 0$ C/m^2 and $\mathcal{B}_{z_t} = \mathcal{B}_{z_b} = 0$ T conditions are imposed at external surfaces for the open circuit case (OC); $\phi_t = \phi_b = 0$ V and $\psi_t = \psi_b = 0$ V conditions at external surfaces are valid for the closed circuit case (CC). Elastic, electric and magnetic properties of *Adaptive Wood* and *Composite* materials are given in Table 1. Table 7 (for closed circuit configuration) and Table 8 (for open circuit configuration) show the first five circular frequencies $\bar{\omega}$ for different half-wave number couples (m, n) and several a/h thickness ratios. When the thickness ratio a/h increases, the circular frequency $\bar{\omega}$ decreases because the stiffness of the flat panel is smaller. For thickness ratio a/h fixed and (m, n) imposed, the circular frequency $\bar{\omega}$ values increase going from the first (I) to the fifth (V) vibration mode. When the vibration mode is fixed (e.g., the first (I) one), the frequency value increases when the half-wave number increases. The behavior of the structure in terms of frequency evaluations, thickness ratio effects, vibration modes through the thickness direction and half-wave number couples (m, m) is the same for both open (OC) and closed circuit (CC) configurations. Frequency values for CC and OC configurations are very similar even if bigger differences are shown for thicker plates and higher values of m and n. These differences remain similar even when the vibration mode order changes. In Figs. 2 and 3, the first three vibration modes are shown for the closed circuit configuration in terms of normalized displacement u^*, v^* and w^*, normalized potentials ϕ^* and ψ^*, normalized transverse normal stress σ^*_{zz}, normalized transverse normal magnetic induction $\mathcal{B}^*_z$ and normalized transverse normal electric displacement $\mathcal{D}^*_z$. Fig. 2 considers a thick plate ($a/h = 4$) and imposed half-wave numbers equal to $m = 1$ and $n = 1$. For each vibration mode, the zigzag effect for each electro-magneto-elastic variable is clearly shown because the analyzed structure has a high transverse anisotropy. The continuity of each variable at interfaces

is obtained because the interlaminar continuity has been correctly imposed. The free vibration analysis is in closed circuit configuration: transverse normal stress σ_{zz}^{*} is zero at external surfaces, electric potential ϕ^{*} and magnetic potential ψ^{*} are zero at external surfaces and transverse normal electric displacement $\mathcal{D}_{z}^{*}$ and magnetic induction $\mathcal{B}_{z}^{*}$ are free (they are different from zero at external surfaces). Fig. 3 considers a thinner flat panel ($a/h = 50$) with imposed half-wave numbers equal to $m = 1$ and $n = 2$. This thinner structure is analyzed in closed circuit configuration too. Fig. 2 shows that the I vibration mode is purely flexural because w^{*} has a constant value and u^{*} and v^{*} have antisymmetric linear trends along the thickness direction. The II and III vibration modes are purely membranal because u^{*} and v^{*} are linear symmetric and w^{*} has an antisymmetric trend along the thickness direction. For both thickness ratios, the peak of σ_{zz}^{*} for the I vibration mode occurs in correspondence with the interface where material changes from *Adaptive Wood* to *Composite*. For II and III vibration modes, the maximum value of σ_{zz}^{*} is reached within one of the *Composite* lamina. In Fig. 3, the thinner plate configuration shows in a clearer way that the I vibration mode is flexural and II and III vibration modes are membranal. Comparisons between Fig. 3 (thinner plate) and Fig. 2 (thicker plate) show a clear thickness layer effect. For the closed circuit case, ϕ^{*} and ψ^{*} have different behaviors and magnitudes for each proposed thickness ratio. This feature shows the different influence of the two physical fields in the behavior of the flat panel. The same considerations remain valid for $\mathcal{D}_{z}^{*}$ and $\mathcal{B}_{z}^{*}$; they have similar trends along the thickness direction but with different magnitudes. This feature certifies the different amplitudes of magnetic and electric fields applied to the structure for the three different vibration modes. Figs. 4 and 5 give the same study for the open circuit configuration. Fig. 4 shows a thick plate ($a/h = 10$) case for imposed half-wave numbers $m = 3$ and $n = 2$. For each vibration mode, zigzag effects for electro-magneto-elastic variables and interlaminar continuity conditions are confirmed. However, in open circuit configuration there are several differences and some similarities: transverse normal stress σ_{zz}^{*} is still zero at external surfaces; electric potential ϕ^{*} and magnetic potential ψ^{*} are now different from zero at external surfaces; transverse normal electric displacement $\mathcal{D}_{z}^{*}$ and transverse normal magnetic induction $\mathcal{B}_{z}^{*}$ are zero at external surfaces. Fig. 5 shows a thin plate ($a/h = 100$) case for imposed half-wave numbers $m = 2$ and $n = 2$. This thin structure is analyzed in open circuit configuration. Therefore, all the features described for the thick structure are here confirmed. Figs. 4–5 show the three displacement trends for the first three vibration modes: the I vibration mode is flexural, II and III vibration modes are classical membranal for both $a/h = 10$ and $a/h = 100$ thickness ratios. Electric potential ϕ^{*} and magnetic potential ψ^{*} have opposite behavior for both thick and thin structures. Maximum values for ϕ^{*} and ψ^{*} are shown at the top and bottom of the flat panel for each investigated thickness ratio. Transverse normal stress σ_{zz}^{*} for the I vibration mode has its maximum value at the interface between the two materials. In the cases of II and III vibration mode, the maximum value is shown in the *Composite* laminated core. Transverse normal electric displacement $\mathcal{D}_{z}^{*}$ and transverse normal magnetic induction $\mathcal{B}_{z}^{*}$ have similar trends along the thickness direction but with different magnitudes. This feature means that they have a different influence on the free vibration behavior of the flat panel. The maximum value for these two variables is always shown at the interface between the two different materials. Fig. 4 shows a bigger zigzag effect along the thickness direction because the plate is thicker.

Table 7: Benchmark (CC), simply supported layered electro-magneto-elastic square flat panel in closed circuit configuration. 3D-u-ϕ-ψ model for free vibration analysis

	$\bar{\omega} = \omega/100$				
a/h	4	10	20	50	100
(1,1)-I	42.848	32.684	21.212	9.4756	4.8249

(Continued)

Table 7 (continued)

$\bar{\omega} = \omega/100$					
(1,1)-II	187.20	204.12	207.41	208.39	208.53
(1,1)-III	206.16	293.11	297.81	299.02	299.19
(1,1)-IV	218.63	340.28	605.11	1452.6	2884.6
(1,1)-V	267.69	440.25	671.57	1498.8	2945.0
(1,2)-I	69.491	59.218	43.290	21.086	10.931
(1,2)-II	223.74	273.22	281.01	284.35	284.90
(1,2)-III	252.38	398.14	453.92	459.55	460.35
(1,2)-IV	284.59	432.65	643.25	1479.0	2904.1
(1,2)-V	325.07	526.80	735.53	1520.0	2950.0
(2,1)-I	75.469	63.888	49.204	25.850	13.682
(2,1)-II	214.92	242.47	246.31	247.45	247.61
(2,1)-III	237.29	369.51	548.39	555.92	556.90
(2,1)-IV	242.24	502.69	622.29	1458.7	2887.5
(2,1)-V	344.16	577.67	846.44	1586.8	2991.0
(2,2)-I	93.455	82.137	65.369	35.470	18.951
(2,2)-II	229.65	387.03	408.24	415.65	416.78
(2,2)-III	317.22	452.92	586.22	596.67	598.04
(2,2)-IV	318.09	520.16	680.56	1487.8	2905.1
(2,2)-V	363.53	594.20	880.50	1604.0	2997.7
(3,1)-I	112.98	99.131	82.652	50.304	28.128
(3,1)-II	236.14	284.21	289.14	290.83	291.09
(3,1)-III	270.92	409.94	648.49	823.64	826.67
(3,1)-IV	288.89	551.59	796.61	1470.0	2893.1
(3,1)-V	379.73	619.34	1075.9	1722.1	3065.4
(3,2)-I	125.74	112.38	94.969	58.440	32.847
(3,2)-II	242.23	423.62	448.81	456.76	457.93
(3,2)-III	342.49	486.40	707.58	843.57	847.37
(3,2)-IV	347.83	553.21	810.27	1499.5	2909.8
(3,2)-V	409.70	714.49	1098.8	1737.1	3072.7

Table 8: Benchmark (OC), simply supported layered electro-magneto-elastic square flat panel in open circuit configuration. 3D-u-ϕ-ψ model for free vibration analysis

$\bar{\omega} = \omega/100$					
a/h	**4**	**10**	**20**	**50**	**100**
(1,1)-I	42.855	32.687	21.212	9.4757	4.8249
(1,1)-II	187.21	204.12	207.41	208.39	208.54
(1,1)-III	206.16	293.12	297.83	299.04	299.21
(1,1)-IV	218.63	340.28	605.12	1452.6	2884.8

(Continued)

Table 8 (continued)

	$\bar{\omega} = \omega/100$				
(1,1)-V	267.69	440.29	671.63	1499.0	2945.2
(1,2)-I	69.507	59.225	43.292	21.087	10.931
(1,2)-II	223.74	273.22	281.01	284.36	284.90
(1,2)-III	252.38	398.15	453.94	459.58	460.39
(1,2)-IV	284.61	432.65	643.25	1479.0	2904.3
(1,2)-V	325.09	526.82	735.59	1520.2	2950.1
(2,1)-I	75.493	63.895	49.206	25.850	13.682
(2,1)-II	214.93	242.47	246.31	247.45	247.62
(2,1)-III	237.31	369.52	548.41	555.95	556.93
(2,1)-IV	242.28	502.69	622.29	1458.7	2887.6
(2,1)-V	344.17	577.68	846.55	1587.0	2991.3
(2,2)-I	93.490	82.149	65.373	35.470	18.951
(2,2)-II	229.65	387.04	408.24	415.66	416.79
(2,2)-III	317.28	452.93	586.24	596.70	598.09
(2,2)-IV	318.15	520.16	680.56	1487.8	2905.2
(2,2)-V	363.55	594.20	880.57	1604.1	2997.9
(3,1)-I	113.05	99.146	82.657	50.305	28.128
(3,1)-II	236.16	284.21	289.14	290.84	291.10
(3,1)-III	270.97	409.95	648.49	823.68	826.71
(3,1)-IV	288.93	551.59	796.65	1470.0	2893.1
(3,1)-V	379.75	619.34	1076.1	1722.3	3065.7
(3,2)-I	125.81	112.40	94.977	58.442	32.847
(3,2)-II	242.26	423.64	448.81	456.77	457.95
(3,2)-III	342.56	486.43	707.58	843.61	847.42
(3,2)-IV	347.93	553.21	810.29	1499.5	2909.8
(3,2)-V	409.71	714.49	1099.0	1737.3	3073.0

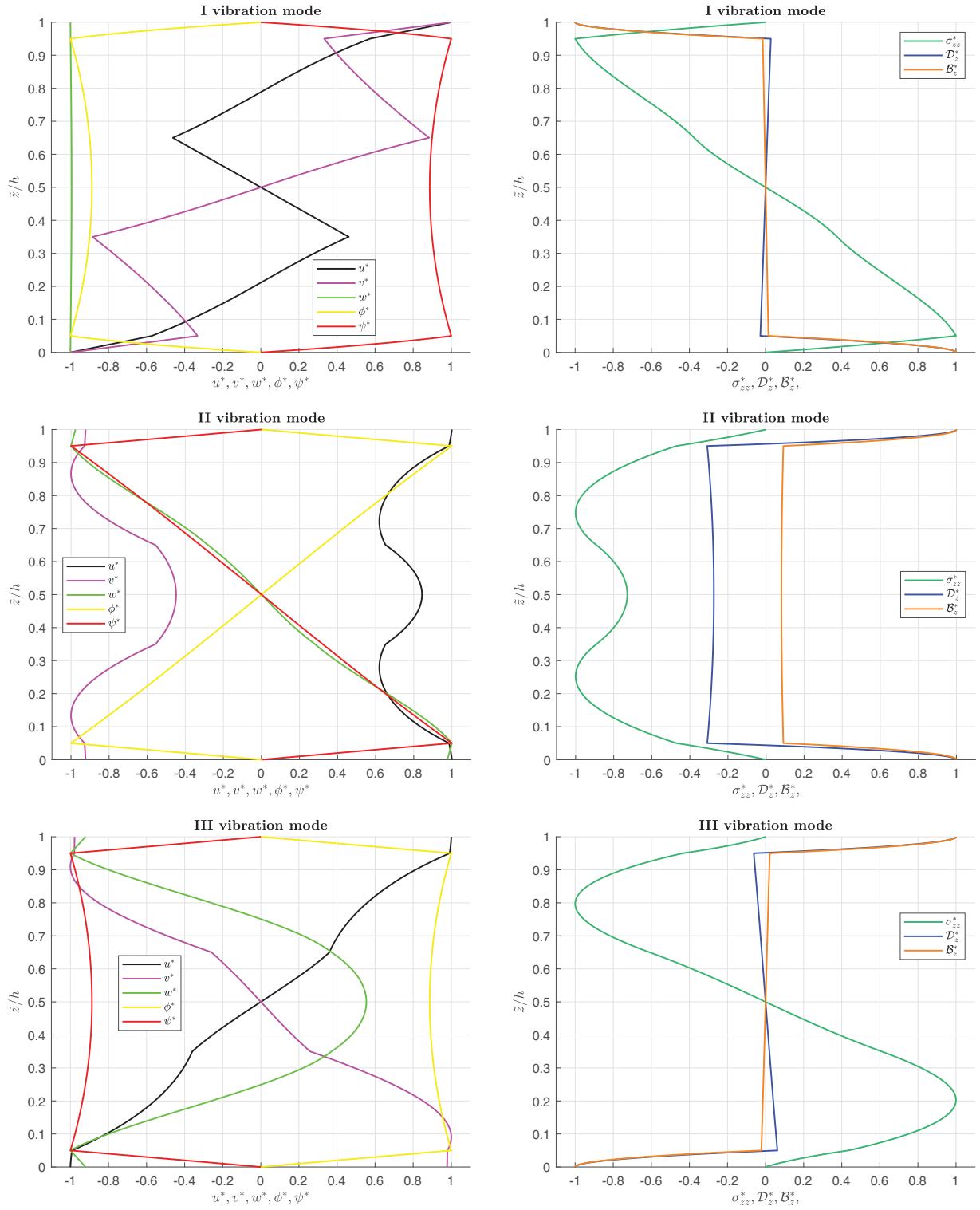

Figure 2: Benchmark (CC), simply-supported layered square flat panel in closed circuit configuration. Thickness ratio a/h = 4. First three vibration modes through the thickness direction for m = 1 and n = 1

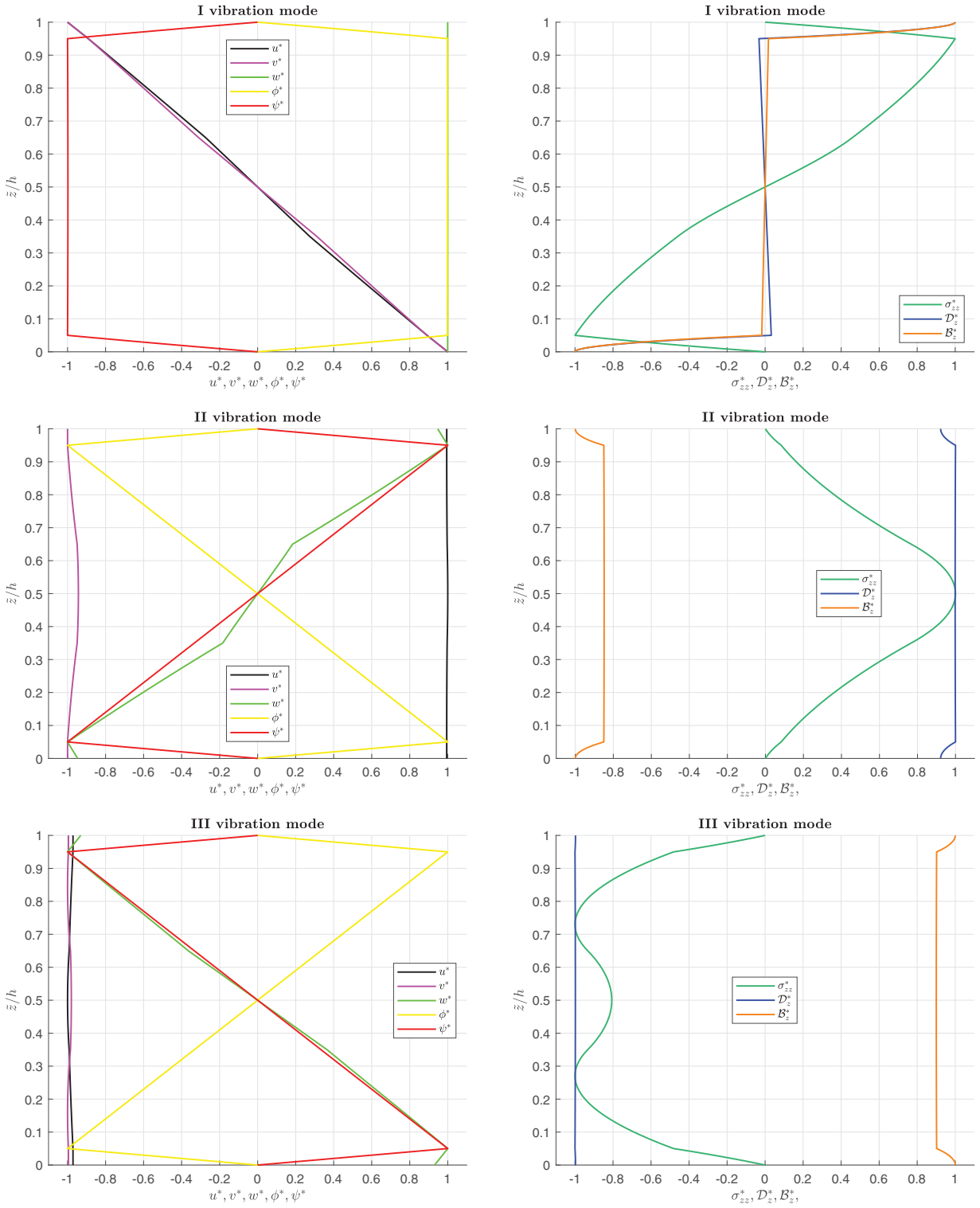

Figure 3: Benchmark (CC), simply-supported layered square flat panel in closed circuit configuration. Thickness ratio a/h = 50. First three vibration modes through the thickness direction for m = 1 and n = 2

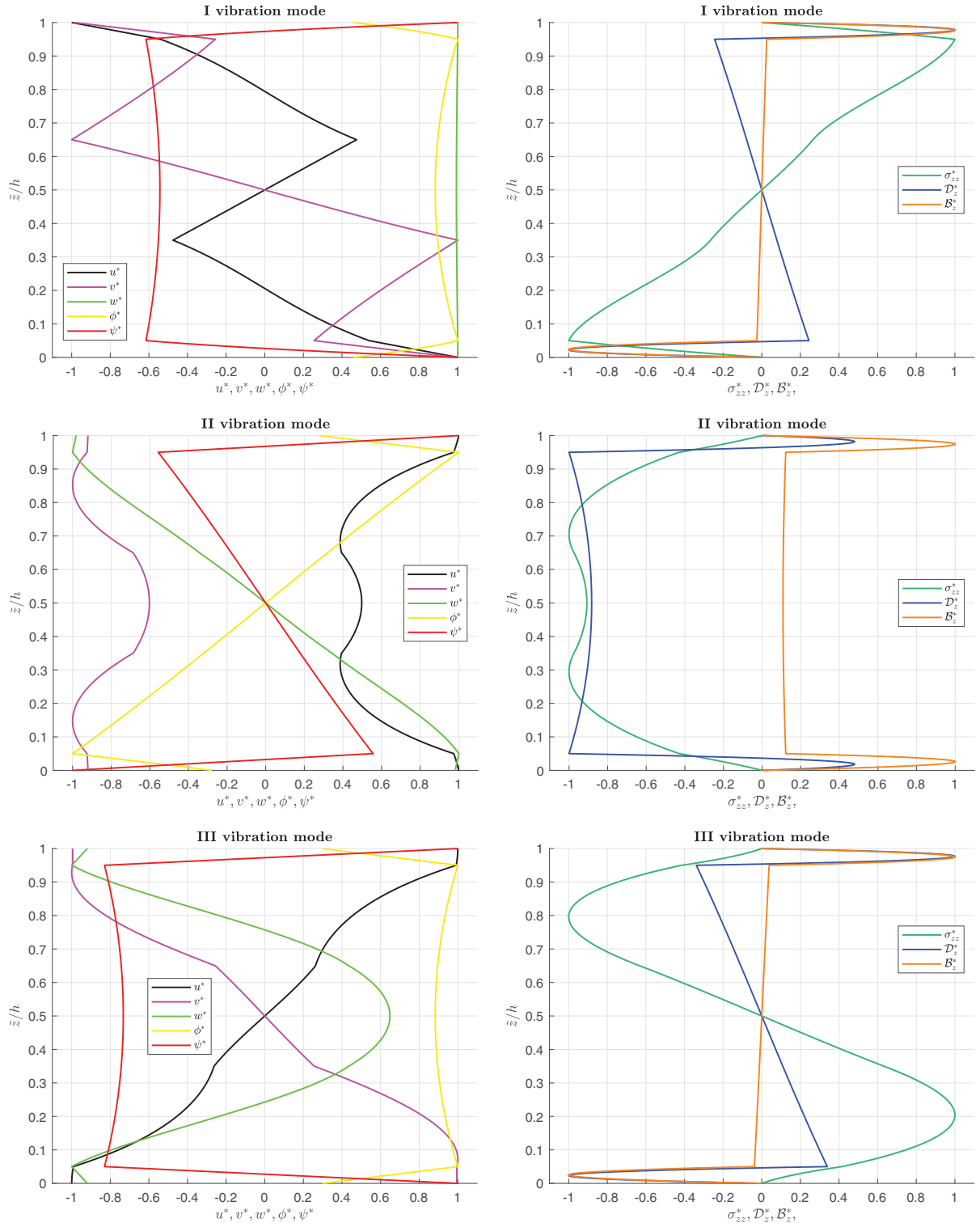

Figure 4: Benchmark (OC), simply-supported layered square flat panel in open circuit configuration. Thickness ratio a/h = 10. First three vibration modes through the thickness direction for m = 3 and n = 2

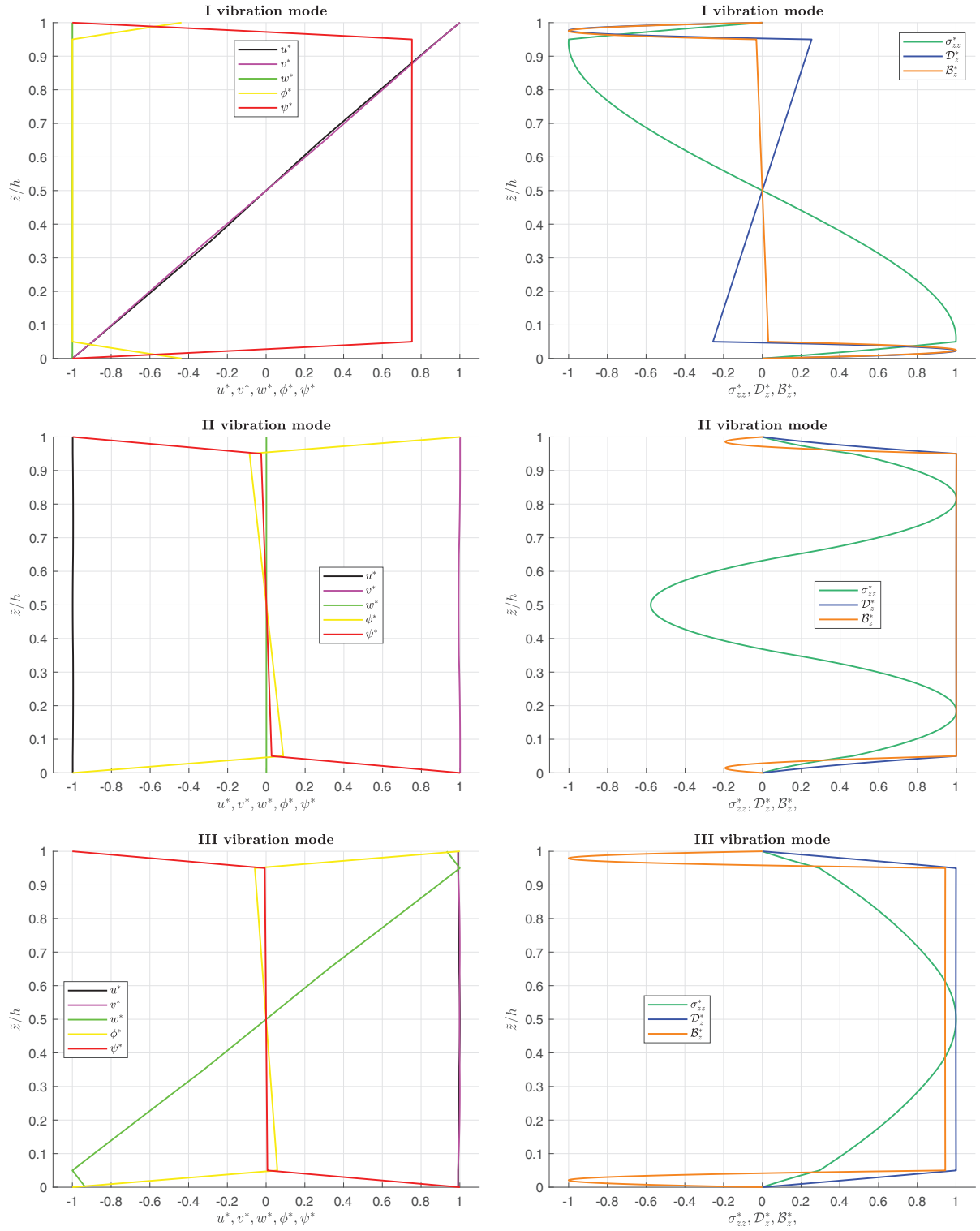

Figure 5: Benchmark (OC), simply-supported layered square flat panel in open circuit configuration. Thickness ratio a/h = 100. First three vibration modes through the thickness direction for m = 2 and n = 2

4 Conclusions

The present paper shows a 3D analytical formulation, which couples magnetic, electric and elastic fields for the free vibration analysis of simply supported flat panels. The set of five second-order differential equations for plates involves the 3D equations of motion, the 3D divergence equation for the magnetic induction and the 3D divergence equation for the electric displacement. Solution method invokes the Navier harmonic forms in the planar directions and the exponential matrix method in the transverse direction. A closed-form solution is employed: simply supported constraint conditions and isotropic or orthotropic materials are required. A layer-wise approach is implemented considering interlaminar continuity conditions in correspondence of two subsequent layers in terms of displacements, electric and magnetic potential, transverse shear and transverse normal stresses, transverse normal magnetic induction/electric displacement. In the assessments, the present 3D magneto-electro-elastic model is validated by comparing separately the results from the 3D electro-elastic model and a 3D magneto-elastic model. Comparisons with 3D electro-magneto-elastic models are also proposed. Both open and closed-circuit configurations are validated considering different thickness ratios (from thick to thin structures) and different half-wave number couples. Assessments allow the validation of the electro-elastic coupling, the magneto-elastic coupling and the electro-magneto-elastic coupling. In the new benchmark, a new plate case is proposed where the full coupling between magnetic, electric and elastic fields is considered. Circular frequency values in open and closed circuit configurations are collected in tabular form for different thickness ratios, half-wave numbers, and vibration mode orders. Circular frequencies decrease when the plate is thinner. The frequency values increase from the first to the fifth mode when the half-wave number couple is fixed. The frequency increases when the half-wave numbers increase for a given vibration mode. The open circuit configuration always gives frequency values bigger than the closed circuit configuration, even if these differences are very small. In figures for vibration modes through the thickness direction, the zigzag effect and the interlaminar continuity (connected with the transverse anisotropy) are clearly shown. Moreover, the model can correctly consider the boundary conditions related to the free vibration analysis for both open and closed circuit configurations. Future developments will consider the addition of thermal and hygroscopic fields to the proposed three-field model.

Acknowledgement: Not applicable.

Funding Statement: The authors received no specific funding for this study.

Author Contributions: The authors confirm contribution to the paper as follows: Conceptualization, Salvatore Brischetto and Domenico Cesare; methodology, Salvatore Brischetto; software, Tommaso Mondino; validation, Tommaso Mondino; formal analysis, Domenico Cesare and Tommaso Mondino; investigation, Domenico Cesare and Tommaso Mondino; resources, Salvatore Brischetto; data curation, Tommaso Mondino; writing—original draft preparation, Domenico Cesare; writing—review and editing, Salvatore Brischetto; visualization, Domenico Cesare; supervision, Salvatore Brischetto; project administration, Salvatore Brischetto; funding acquisition, Salvatore Brischetto. All authors reviewed the results and approved the final version of the manuscript.

Availability of Data and Materials: Not applicable.

Ethics Approval: Not applicable.

Conflicts of Interest: The authors declare no conflicts of interest to report regarding the present study.

Appendix A

Meaning of P_i^k terms in Eq. (14a):

$$P_1^k = A_{31}^k\left(A_{43}^kA_{55}^k - A_{44}^kA_{54}^k\right) - A_{32}^k\left(A_{42}^kA_{55}^k - A_{44}^kA_{53}^k\right) + A_{33}^k\left(A_{42}^kA_{54}^k - A_{43}^kA_{53}^k\right), \tag{A1}$$

$$P_2^k = A_{43}^kA_{55}^kA_{21}^k - A_{44}^kA_{54}^kA_{21}^k - A_{32}^kA_{55}^kA_{34}^k + A_{32}^kA_{44}^kA_{45}^k + A_{33}^kA_{54}^kA_{34}^k - A_{33}^kA_{43}^kA_{45}^k, \tag{A2}$$

$$P_3^k = A_{43}^kA_{55}^kA_{22}^k - A_{44}^kA_{54}^kA_{22}^k - A_{32}^kA_{55}^kA_{35}^k + A_{32}^kA_{44}^kA_{46}^k + A_{33}^kA_{54}^kA_{35}^k - A_{33}^kA_{43}^kA_{46}^k, \tag{A3}$$

$$P_4^k = A_{43}^kA_{55}^kA_{23}^k - A_{44}^kA_{54}^kA_{23}^k - A_{32}^kA_{55}^kA_{36}^k + A_{32}^kA_{44}^kA_{47}^k + A_{33}^kA_{54}^kA_{36}^k - A_{33}^kA_{43}^kA_{47}^k, \tag{A4}$$

$$P_5^k = A_{43}^kA_{55}^kA_{24}^k - A_{44}^kA_{54}^kA_{24}^k - A_{32}^kA_{55}^kA_{37}^k + A_{32}^kA_{44}^kA_{48}^k + A_{33}^kA_{54}^kA_{37}^k - A_{33}^kA_{43}^kA_{48}^k, \tag{A5}$$

$$P_6^k = A_{43}^kA_{55}^kA_{25}^k - A_{44}^kA_{54}^kA_{25}^k - A_{32}^kA_{55}^kA_{38}^k + A_{32}^kA_{44}^kA_{49}^k + A_{33}^kA_{54}^kA_{38}^k - A_{33}^kA_{43}^kA_{49}^k, \tag{A6}$$

$$P_7^k = A_{43}^kA_{55}^kA_{26}^k - A_{44}^kA_{54}^kA_{26}^k - A_{32}^kA_{55}^kA_{39}^k + A_{32}^kA_{44}^kA_{50}^k + A_{33}^kA_{54}^kA_{39}^k - A_{33}^kA_{43}^kA_{50}^k, \tag{A7}$$

$$P_8^k = A_{43}^kA_{55}^kA_{27}^k - A_{44}^kA_{54}^kA_{27}^k - A_{32}^kA_{55}^kA_{40}^k + A_{32}^kA_{44}^kA_{51}^k + A_{33}^kA_{54}^kA_{40}^k - A_{33}^kA_{43}^kA_{51}^k, \tag{A8}$$

$$P_9^k = A_{43}^kA_{55}^kA_{28}^k - A_{44}^kA_{54}^kA_{28}^k - A_{32}^kA_{55}^kA_{41}^k + A_{32}^kA_{44}^kA_{52}^k + A_{33}^kA_{54}^kA_{41}^k - A_{33}^kA_{43}^kA_{52}^k, \tag{A9}$$

$$P_{10}^k = A_{43}^kA_{55}^kA_{29}^k - A_{44}^kA_{54}^kA_{29}^k, \tag{A10}$$

$$P_{11}^k = A_{43}^kA_{55}^kA_{30}^k - A_{44}^kA_{54}^kA_{30}^k, \tag{A11}$$

$$P_{12}^k = A_{31}^kA_{55}^kA_{34}^k - A_{31}^kA_{44}^kA_{45}^k - A_{42}^kA_{55}^kA_{21}^k + A_{44}^kA_{53}^kA_{21}^k + A_{33}^kA_{42}^kA_{45}^k - A_{33}^kA_{53}^kA_{34}^k, \tag{A12}$$

$$P_{13}^k = A_{31}^kA_{55}^kA_{35}^k - A_{31}^kA_{44}^kA_{46}^k - A_{42}^kA_{55}^kA_{22}^k + A_{44}^kA_{53}^kA_{22}^k + A_{33}^kA_{42}^kA_{46}^k - A_{33}^kA_{53}^kA_{35}^k, \tag{A13}$$

$$P_{14}^k = A_{31}^kA_{55}^kA_{36}^k - A_{31}^kA_{44}^kA_{47}^k - A_{42}^kA_{55}^kA_{23}^k + A_{44}^kA_{53}^kA_{22}^k + A_{33}^kA_{42}^kA_{47}^k - A_{33}^kA_{53}^kA_{36}^k, \tag{A14}$$

$$P_{15}^k = A_{31}^kA_{55}^kA_{37}^k - A_{31}^kA_{44}^kA_{48}^k - A_{42}^kA_{55}^kA_{24}^k + A_{44}^kA_{53}^kA_{22}^k + A_{33}^kA_{42}^kA_{48}^k - A_{33}^kA_{53}^kA_{37}^k, \tag{A15}$$

$$P_{16}^k = A_{31}^kA_{55}^kA_{38}^k - A_{31}^kA_{44}^kA_{49}^k - A_{42}^kA_{55}^kA_{25}^k + A_{44}^kA_{53}^kA_{22}^k + A_{33}^kA_{42}^kA_{49}^k - A_{33}^kA_{53}^kA_{38}^k, \tag{A16}$$

$$P_{17}^k = A_{31}^kA_{55}^kA_{39}^k - A_{31}^kA_{44}^kA_{50}^k - A_{42}^kA_{55}^kA_{26}^k + A_{44}^kA_{53}^kA_{22}^k + A_{33}^kA_{42}^kA_{50}^k - A_{33}^kA_{53}^kA_{39}^k, \tag{A17}$$

$$P_{18}^k = A_{31}^kA_{55}^kA_{40}^k - A_{31}^kA_{44}^kA_{51}^k - A_{42}^kA_{55}^kA_{27}^k + A_{44}^kA_{53}^kA_{22}^k + A_{33}^kA_{42}^kA_{51}^k - A_{33}^kA_{53}^kA_{40}^k, \tag{A18}$$

$$P_{19}^k = A_{31}^kA_{55}^kA_{41}^k - A_{31}^kA_{44}^kA_{52}^k - A_{42}^kA_{55}^kA_{28}^k + A_{44}^kA_{53}^kA_{22}^k + A_{33}^kA_{42}^kA_{52}^k - A_{33}^kA_{53}^kA_{41}^k, \tag{A19}$$

$$P_{20}^k = -A_{42}^kA_{55}^kA_{29}^k + A_{44}^kA_{53}^kA_{22}^k, \tag{A20}$$

$$P_{21}^k = -A_{42}^kA_{55}^kA_{30}^k + A_{44}^kA_{53}^kA_{22}^k, \tag{A21}$$

$$P_{22}^k = A_{31}^kA_{43}^kA_{45}^k - A_{31}^kA_{54}^kA_{34}^k - A_{32}^kA_{42}^kA_{45}^k + A_{32}^kA_{53}^kA_{34}^k + A_{42}^kA_{54}^kA_{21}^k - A_{43}^kA_{53}^kA_{21}^k, \tag{A22}$$

$$P_{23}^k = A_{31}^kA_{43}^kA_{46}^k - A_{31}^kA_{54}^kA_{35}^k - A_{32}^kA_{42}^kA_{46}^k + A_{32}^kA_{53}^kA_{35}^k + A_{42}^kA_{54}^kA_{22}^k - A_{43}^kA_{53}^kA_{22}^k, \tag{A23}$$

$$P_{24}^k = A_{31}^kA_{43}^kA_{47}^k - A_{31}^kA_{54}^kA_{36}^k - A_{32}^kA_{42}^kA_{47}^k + A_{32}^kA_{53}^kA_{36}^k + A_{42}^kA_{54}^kA_{23}^k - A_{43}^kA_{53}^kA_{23}^k, \tag{A24}$$

$$P_{25}^k = A_{31}^kA_{43}^kA_{48}^k - A_{31}^kA_{54}^kA_{37}^k - A_{32}^kA_{42}^kA_{48}^k + A_{32}^kA_{53}^kA_{37}^k + A_{42}^kA_{54}^kA_{24}^k - A_{43}^kA_{53}^kA_{24}^k, \tag{A25}$$

$$P_{26}^k = A_{31}^kA_{43}^kA_{49}^k - A_{31}^kA_{54}^kA_{38}^k - A_{32}^kA_{42}^kA_{49}^k + A_{32}^kA_{53}^kA_{38}^k + A_{42}^kA_{54}^kA_{25}^k - A_{43}^kA_{53}^kA_{25}^k, \tag{A26}$$

$$P_{27}^k = A_{31}^kA_{43}^kA_{50}^k - A_{31}^kA_{54}^kA_{39}^k - A_{32}^kA_{42}^kA_{50}^k + A_{32}^kA_{53}^kA_{39}^k + A_{42}^kA_{54}^kA_{26}^k - A_{43}^kA_{53}^kA_{26}^k, \tag{A27}$$

$$P_{28}^k = A_{31}^kA_{43}^kA_{51}^k - A_{31}^kA_{54}^kA_{40}^k - A_{32}^kA_{42}^kA_{51}^k + A_{32}^kA_{53}^kA_{40}^k + A_{42}^kA_{54}^kA_{27}^k - A_{43}^kA_{53}^kA_{27}^k, \tag{A28}$$

$$P_{29}^k = A_{31}^kA_{43}^kA_{52}^k - A_{31}^kA_{54}^kA_{41}^k - A_{32}^kA_{42}^kA_{52}^k + A_{32}^kA_{53}^kA_{41}^k + A_{42}^kA_{54}^kA_{28}^k - A_{43}^kA_{53}^kA_{28}^k, \tag{A29}$$

$$P_{30}^k = A_{42}^kA_{54}^kA_{29}^k - A_{43}^kA_{53}^kA_{29}^k, \tag{A30}$$

$$P_{31}^k = A_{42}^kA_{54}^kA_{30}^k - A_{43}^kA_{53}^kA_{30}^k. \tag{A31}$$

References

1. Tornabene F. Hygro-thermo-magneto-electro-elastic theory of anisotropic doubly-curved shells. In: Higher-order strong andweak formultions for arbitrarily shaped shell structures. Bologna, Italy: Società Editrice Esculapio; 2023.
2. Zhu X. Piezoelectric ceramic materials processing, properties, characterization and applications, materials science and technologies. 1st. Hauppauge, NY, USA: Nova Science Publishers; 2010.
3. Mi X, Zhao Y, Zhan Q, Chen M. Vibration reduction study of a simplified floating raft system by installing connecting nonlinear spring-mass systems. Thin-Walled Struct. 2025;210(3):113015. doi:10.1016/j.tws.2025.113015.
4. Wang S, He J, Fan J, Sun P, Wang D. A time-domain method for free vibration responses of an equivalent viscous damped system based on a complex damping model. J Low Frequency Noise Vib Active Control. 2023;42(3):1531–40. doi:10.1177/14613484231157514.
5. Zhai Y, Li S, Zhang X. Vibration performance of composite doubly curved shells embedded with damping layer. Int J Struct Stab Dyn. 2025. doi:10.1142/S0219455426502652.
6. Zhang X, Liu Y, Chen X, Li Z, Su C-Y. Adaptive pseudoinverse control for constrained hysteretic nonlinear systems and its application on dielectric elastomer actuator. IEEE/ASME Trans Mechatron. 2023;28(4):2142–54. doi:10.1109/tmech.2022.3231263.
7. Ren H, Zhuang X, Rabczuk T. Nonlocal operator method with numerical integration for gradient solid. Comput Struct. 2020;233(1):106235. doi:10.1016/j.compstruc.2020.106235.
8. Carrera E, Gifico MDi, Nali P, Brischetto S. Refined multilayered plate elements for coupled magneto-electro-elastic analysis. Multidiscip Model Mater Struct. 2009;5(2):119–38. doi:10.1163/157361109787959859.
9. Yang ZX, Dang PF, Han QK, Jin ZH. Natural characteristics analysis of magneto-electro-elastic multilayered plate using analytical and finite element method. Compos Struct. 2018;185(3):411–20. doi:10.1016/j.compstruct.2017.11.031.
10. Bhangale RK, Ganesan N. Free vibration of simply supported functionally graded and layered magneto-electro-elastic plates by finite element method. J Sound Vib. 2006;294(4–5):1016–38. doi:10.1016/j.jsv.2005.12.030.
11. Chen JY, Heyliger PR, Pan E. Free vibration of three-dimensional multilayered magneto-electro-elastic plates under combined clamped/free boundary conditions. J Sound Vib. 2014;333(17):4017–29. doi:10.1016/j.jsv.2014.03.035.
12. Jiangong Y, Juncai D, Zhijuan M. On dispersion relations of waves in multilayered magneto-electro-elastic plates. Appl Math Model. 2012;36(12):5780–91. doi:10.1016/j.apm.2012.01.028.
13. Pham Q-H, Tran VK, Nguyen P-C. Dynamic response of magneto-electro-elastic composite plates lying on visco-Pasternak medium subjected to blast load. Compos Struct. 2024;337:118054. doi:10.1016/j.compstruct.2024.118054.
14. Kattimani SC, Ray MC. Smart damping of geometrically nonlinear vibrations of magneto-electro-elastic plates. Compos Struct. 2014;114(5):51–63. doi:10.1016/j.compstruct.2014.03.050.
15. Xu LL, Kang CC, Zheng YF, Chen CP. Analysis of nonlinear vibration of magneto-electro-elastic plate on elastic foundation based on high-order shear deformation. Compos Struct. 2021;271:114149. doi:10.1016/j.compstruct.2021.114149.
16. Vinyas M. A higher-order free vibration analysis of carbon nanotube-reinforced magneto-electro-elastic plates using finite element methods. Compos Part B Eng. 2019;158(4):286–301. doi:10.1016/j.compositesb.2018.09.086.
17. Milazzo A. Variable kinematics models and finite elements for nonlinear analysis of multilayered smart plates. Compos Struct. 2015;122(1):537–45. doi:10.1016/j.compstruct.2014.12.003.
18. Milazzo A. Refined equivalent single layer formulations and finite elements for smart laminates free vibrations. Compos Part B Eng. 2014;61(16):238–53. doi:10.1016/j.compositesb.2014.01.055.
19. Milazzo A. An equivalent single-layer approach for free vibration analysis of smart laminated thick composite plates. Smart Mater Struct. 2012;21:075031.
20. Davì G, Milazzo A. A regular variational boundary model for free vibrations of magneto-electro-elastic structures. Eng Anal Bound Elem. 2011;35(3):303–12. doi:10.1016/j.enganabound.2010.10.004.
21. Vinyas M, Kattimani SC. Finite element evaluation of free vibration characteristics of magneto-electro-elastic rectangular plates in hygrothermal environment using higher-order shear deformation theory. Compos Struct. 2018;202(3):1339–52. doi:10.1016/j.compstruct.2018.06.069.

22. Ramirez F, Heyliger PR, Pan E. Free vibration response of two-dimensional magneto-electro-elastic laminated plates. J Sound Vib. 2006;292(3–5):626–44. doi:10.1016/j.jsv.2005.08.004.
23. Kiran MC, Kattimani SC. Free vibration of multilayered magneto-electro-elastic plates with skewed edges using layer wise shear deformation theory. Mater Today Proc. 2018;5(10):21248–21255. doi:10.1016/j.matpr.2018.06.525.
24. Soni S, Jain NK, Joshi PV. Analytical modeling for nonlinear vibration analysis of partially cracked thin magneto-electro-elastic plate coupled with fluid. Nonlinear Dyn. 2017;90(1):137–70. doi:10.1007/s11071-017-3652-5.
25. Xu L-L, Chen C-P, Zheng Y-F. Two-degrees-of-freedom nonlinear free vibration analysis of magneto-electro-elastic plate based on high order shear deformation theory. Commun Nonlinear Sci Numer Simul. 2022;114:106662. doi:10.1016/j.cnsns.2022.106662.
26. Yang Y, Li X-F. Bending and free vibration of a circular magnetoelectroelastic plate with surface effects. Int J Mech Sci. 2019;157–158(1):858–71. doi:10.1016/j.ijmecsci.2019.05.029.
27. Chen J, Chen H, Pan E, Heyliger PR. Modal analysis of magneto-electro-elastic plates using the state-vector approach. J Sound Vib. 2007;304(3–5):722–34. doi:10.1016/j.jsv.2007.03.021.
28. Chen J, Pan E, Chen H. Wave propagation in magneto-electro-elastic multilayered plates. Int J Solids Strct. 2007;44(3–4):1073–85. doi:10.1016/j.ijsolstr.2006.06.003.
29. Chen J, Guo J, Pan E. Wave propagation in magneto-electro-elastic multilayered plates with nonlocal effect. J Sound Vib. 2017;400:550–63. doi:10.1016/j.jsv.2017.04.001.
30. Pan E, Heyliger PR. Free vibrations of simply supported and multilayered magneto-electro-elastic plates. J Sound Vib. 2002;252(3):429–42. doi:10.1006/jsvi.2001.3693.
31. Dat ND, Quan TQ, Vinyas M, Nguyen DD. Analytical solutions for nonlinear magneto-electro-elastic vibration of smart sandwich plate with carbon nanotube reinforced nanocomposite core in hygrothermal environment. Int J Mech Sci. 2020;186:105906. doi:10.1016/j.ijmecsci.2020.105906.
32. Wang J, Qu L, Qian F. State vector approach of free-vibration analysis of magneto-electro-elastic hybrid laminated plates. Compos Struct. 2010;92(6):1318–24. doi:10.1016/j.compstruct.2009.11.013.
33. Razavi S, Shooshtari A. Nonlinear free vibration of magneto-electro-elastic rectangular plates. Compos Struct. 2015;119(3):377–84. doi:10.1016/j.compstruct.2014.08.034.
34. Xin L, Hu Z. Free vibration of simply supported and multilayered magneto-electro-elastic plates. Compos Struct. 2015;121(6):344–50. doi:10.1016/j.compstruct.2014.11.030.
35. Kuo H-Y, Wang Y-H. Wave motion of magneto-electro-elastic laminated plates with membrane-type interfacial imperfections. Compos Struct. 2022;293:115661. doi:10.1016/j.compstruct.2022.115661.
36. Dinh KN, Duc TV. Vibration analysis of a magneto-electro-elastic sandwich composite plate with a new honeycomb structure core layer in a thermal environment. Aerosp Sci Technol. 2025;157(3):109846. doi:10.1016/j.ast.2024.109846.
37. Hamidi M, Zaki S, Aboussaleh M. Modeling and numerical simulation of the dynamic behavior of magneto-electro-elastic multilayer plates based on aWinkler-Pasternak elastic foundation. J Intell Mater Syst Struct. 2020;32(8):1–15. doi:10.1177/1045389x20969845.
38. Ke L-L, Wang Y-S, Yang J, Kitipornchai S. Free vibration of size-dependent magneto-electro-elastic nanoplates based on the nonlocal theory. Acta Mech Sin. 2014;30(4):516–25. doi:10.1007/s10409-014-0072-3.
39. Li YS, Cai ZY, Shi SY. Buckling and free vibration of magnetoelectroelastic nanoplate based on nonlocal theory. Compos Struct. 2014;111:522–9. doi:10.1016/j.compstruct.2014.01.033.
40. Chang T-P. Free vibration of fluid-loaded transversely isotropic magneto-electro-elastic plates. Appl Mech Mater. 2013;284–287:758–62. doi:10.4028/www.scientific.net/amm.284-287.758.
41. Jamalpoor A, Ahmadi-Savadkoohi A, Hosseini-Hashemi S. Free vibration and biaxial buckling analysis of magneto-electro-elastic microplate resting on visco-Pasternak substrate via modified strain gradient theory. Smart Mater Struct. 2016;25(10):105035. doi:10.1088/0964-1726/25/10/105035.
42. Shooshtari A, Razavi S. Vibration of a multiphase magneto-electro-elastic simply supported rectangular plate subjected to harmonic forces. J Intell Mater Syst Struct. 2016;28(4):451–67. doi:10.1177/1045389x16649451.
43. Brischetto S, Cesare D. Three-dimensional vibration analysis of multilayered composite and functionally graded piezoelectric plates and shells. Compos Struct. 2024;346(1):118413. doi:10.1016/j.compstruct.2024.118413.

44. Brischetto S, Cesare D. A 3D shell model for static and free vibration analysis of multilayered magneto-elastic structures. Thin-Walled Struct. 2025;206(7):112620. doi:10.1016/j.tws.2024.112620.
45. Brischetto S. An exact 3D solution for free vibrations of multilayered cross-ply composite and sandwich plates and shells. Int J Appl Mech. 2014;6(6):1450076. doi:10.1142/s1758825114500768.
46. Povstenko Y. Fractional thermoelasticity. Cham, Switzerland: Springer International Publishing; 2015.
47. Boyce WE, DiPrima RC. Elementary differential equations and boundary value problems. New York, NY, USA: John Wiley & Sons, Ltd.; 2001.
48. Reddy JN. Mechanics of laminated composite plates and shells. In: Theory and analysis. Boca Raton, FL, USA: CRC Press; 2014.
49. Chen WQ, Lee KY, Ding HJ. On free vibration of non-homogeneous transversely isotropic magneto-electro-elastic plates. J Sound Vib. 2005;279(1–2):237–51. doi:10.1016/j.jsv.2003.10.033.
50. Pan E. Three-dimensional Green's functions in anisotropic magneto-electro-elastic bimaterials. Zeitschrift Fur Angewandte Mathematik Und Physik ZAMP. 2002;53:815–38.